J. Fluid Mech. (2000), *vol.* 407, *pp.* 315–349. Printed in the United Kingdom

A scalar subgrid model with flow structure for large-eddy simulations of scalar variances

By P. FLOHR† AND J. C. VASSILICOS

Department of Applied Mathematics and Theoretical Physics, University of Cambridge, Silver Street, Cambridge CB3 9EW, UK

(Received 24 June 1998 and in revised form 15 November 1999)

A new model to simulate passive scalar fields in large-eddy simulations of turbulence is presented. The scalar field is described by clouds of tracer particles and the subgrid contribution of the tracer displacement is modelled by a kinematic model which obeys Kolmogorov's inertial-range scaling, is incompressible and incorporates turbulent-like flow structure of the turbulent small scales. This makes it possible to study the scalar variance field with inertial-range effects explicitly resolved by the kinematic subgrid field while the LES determines the value of the Lagrangian integral time scale T_L. In this way, the modelling approach does not rely on unknown Lagrangian input parameters which determine the absolute value of the scalar variance.

The mean separation of particle pairs displays a well-defined Richardson scaling in the inertial range, and we find that the Richardson constant $G_\Delta \approx 0.07$ which is small compared to the value obtained from stochastic models with the same T_L. The probability density function of the separation of particle pairs is found to be highly non-Gaussian in the inertial range of times and for long times becomes Gaussian. We compute the scalar variance field for an instantaneous line source and find good agreement with experimental data.

1. Introduction

1.1. *Overview*

Large-eddy simulation (LES) has become an established tool for the calculation of turbulent flows in simple geometries and is being used in configurations of increasing complexity and practical interest (for a recent overview see, for example, Métais & Ferziger 1997). An important aspect of LES is the transport of passive scalar fields, and in the context of simulations of the planetary boundary layer in particular, the characteristics of scalar transport have been extensively investigated (Ciofalo 1994). In fact, classical and current approaches to LES of scalar fields allow only for the computation of the average concentration field. However, important properties such as mixing rates or possible peak concentrations are related to the concentration variance field, itself determined to a large extent by subgrid turbulent motions, and in this paper we seek a subgrid model that allows us to predict the concentration variance field.

In LES, the turbulent field is decomposed by filtering the equations of motion into a turbulent large-scale field which is explicitly computed and a turbulent small-scale field which is modelled. In the limit of very high Reynolds numbers, models of the subgrid scales are usually based on the assumptions (i) that an inertial range of scales

† Present address: ABB Alstom Technology Ltd., CH-5405 Baden-Daettwil.

exists (where energy is transferred locally in wavenumber space from scale to scale and dissipation is independent of viscosity) and (ii) that the filter acts in the inertial range. Under these assumptions, the effect of the small scales on the mean field may be expected to be mainly one of dissipation and independent of the particular flow configuration. Thus, in analogy with molecular diffusion, one makes a gradient-diffusion assumption and introduces an eddy viscosity ν_t that takes into account the dissipation by the unresolved small scales. The eddy viscosity can then be determined by a direct application of Kolmogorov's universal inertial-range scaling theory.

The simulation of passive scalar fields in LES has mostly relied on an analogous gradient-diffusion assumption for the scalar transport equation, leading to a turbulent diffusivity κ_t which takes into account the turbulent scalar fluctuations at the subgrid scales (Lesieur & Métais 1996). An application of Obukhov–Corrsin's inertial range theory for turbulent scalars then leads to a universally constant turbulent Prandtl number $Pr_t = \nu_t/\kappa_t$ which allows the turbulent diffusivity to be directly computed from the subgrid model of the velocity field.

In this paper, we argue that the turbulent diffusivity κ_t is not appropriate for two reasons. First, even though the derivation of Pr_t (see § 1.2) leads to a constant turbulent Prandtl number, different values for Pr_t have been proposed in the literature ($Pr_t = 0.1 \ldots 1$) so that Pr_t turns out, in practice, to be a variable fit parameter to match reference results (Ciofalo 1994). The second reason why the turbulent diffusivity approach is not appropriate here is that we want to compute scalar variances, and the scalar variance strongly depends on the small-scale turbulent flow structure which a turbulent diffusivity κ_t does not take into account. We therefore seek a way to incorporate the effects of subgrid flow structure on scalar dispersion, and the approach adopted here is Lagrangian and is based on the relation between the Eulerian scalar field and Lagrangian trajectories of marked fluid elements (also referred to as particles in this paper). The only currently available Lagrangian model of turbulent dispersion that is incompressible by construction, incorporates spatio-temporal flow structure and obeys certain fundamental turbulence statistical scalings such as Kolmogorov's $-\frac{5}{3}$ law is Kinematic Simulation (KS) (see Fung *et al.* 1992; Fung & Vassilicos 1998; Malik & Vassilicos 1999). In this paper we use KS to model the spatio-temporal structure of the velocity field that advects the scalar field (or fluid elements) below the grid.

Lagrangian calculations of average concentrations require knowledge of one-particle statistics, and Lagrangian calculations of scalar fluctuations and scalar variances require knowledge of two-particle statistics (Durbin 1980). Recently, one-particle statistics have been used to describe the mean concentration field of plumes in LES of the atmospheric boundary layer (e.g. Hadfield 1994). However, the fluid element trajectories used in the subgrid scales of this LES were generated by Wiener processes. Such one-particle stochastic Lagrangian models of the subgrid scales can only be used to calculate the mean scalar field. But the point here is that it is often of crucial importance to be able to describe the scalar fluctuation field, for example in the prediction of air pollution or the determination of turbulent reaction rates. These quantities are intimately related to the probability distribution function (p.d.f.) of the two-particle separation vector (as discussed in § 2) and Richardson's constant G_Δ (see § 3). To date, no LES of scalar fields has been able to make predictions of the scalar fluctuation field, p.d.f.s of two-particle separations or Richardson's constant. A small Richardson constant implies a large concentration variance, and the issue of whether the separation p.d.f. is Gaussian or not dates back to Batchelor (1952) and Richardson (1926). All these questions and issues are directly addressed in this paper.

In the remainder of this Introduction, we review the concepts of LES and of eddy-viscosity/eddy-diffusivity models in order to highlight the potential drawbacks of the filtering operation and the replacement of the subgrid scales by a simple diffusive process. We then stress the significance of flow structure in the turbulent small scales and compare KS to stochastic models of turbulent dispersion.

1.2. *Eddy-viscosity models in LES*

We only state the definitions and equations that are most relevant to this study. For more detailed information on LES the reader is referred to, for example, Lesieur & Métais (1996).

In LES the relevant flow variables (velocity, pressure, passive scalar) are decomposed into large- and small-scale variables, i.e.

$$\boldsymbol{u} = \overline{\boldsymbol{u}} + \boldsymbol{u}', \quad \theta = \overline{\theta} + \theta', \tag{1.1}$$

where the overbar denotes the filtered (or large-scale) part and the prime denotes the unresolved or small-scale part of the flow field $\boldsymbol{u}$ and passive scalar field θ. The general definition of the filter operation is given by

$$\overline{f}(\boldsymbol{x}) = \int G(\boldsymbol{x} - \boldsymbol{x}') f(\boldsymbol{x}')\, \mathrm{d}\boldsymbol{x}' = \int \hat{G}(\boldsymbol{k}) \hat{f}(\boldsymbol{k}) \exp(\mathrm{i}\boldsymbol{k}\boldsymbol{x})\, \mathrm{d}\boldsymbol{k}, \tag{1.2}$$

where $f(\boldsymbol{x})$ is the variable to be filtered, G is the filter function, and $\hat{f}(\boldsymbol{k})$ and $\hat{G}(\boldsymbol{k})$ are their respective Fourier transforms. In this study we use the sharp Fourier cutoff filter with cutoff wavenumber k_c which is the most straightforward filter to define for spectral LES.

The Navier–Stokes and passive scalar equations for incompressible flow are

$$\partial_t \boldsymbol{u} + (\boldsymbol{u} \cdot \nabla)\boldsymbol{u} = -\nabla p + \nu \nabla^2 \boldsymbol{u}, \tag{1.3}$$

$$\partial_t \theta + \boldsymbol{u} \cdot \nabla \theta = \kappa \nabla^2 \theta, \tag{1.4}$$

with $\nabla \cdot \boldsymbol{u} = 0$, and where ν is the molecular viscosity and κ is the molecular diffusivity. Applying the filter operation to the equations of motion we obtain

$$\partial_t \overline{\boldsymbol{u}} + (\overline{\boldsymbol{u}} \cdot \nabla)\overline{\boldsymbol{u}} = -\nabla \overline{p} + \nu \nabla^2 \overline{\boldsymbol{u}} + \nabla \cdot \boldsymbol{\tau}, \tag{1.5}$$

$$\partial_t \overline{\theta} + \overline{\boldsymbol{u}} \cdot \nabla \overline{\theta} = \kappa \nabla^2 \overline{\theta} + \nabla \boldsymbol{q}, \tag{1.6}$$

where

$$\tau_{ij} = \overline{u}_i \overline{u}_j - \overline{u_i u_j}, \quad q_i = \overline{\theta} \overline{u}_i - \overline{\theta u_i}.$$

The effect of the subgrid scales on the resolved ones appears in the subgrid stress tensor $\boldsymbol{\tau}$ and the subgrid scalar flux $\boldsymbol{q}$. The usual approach to modelling the subgrid fluxes is to make gradient-diffusion assumptions, specifically

$$\tau_{ij} + \delta_{ij}\tau_{kk}/3 = \nu_t(\partial_{x_j}\overline{u}_i + \partial_{x_i}\overline{u}_j), \tag{1.7}$$

$$q_i = \kappa_t \partial_{x_i} \overline{\theta}, \tag{1.8}$$

where the eddy viscosity ν_t and the eddy diffusivity κ_t depend on large-scale variables. For example, the Smagorinsky model relates the eddy viscosity to the large-scale strain tensor, and the spectral eddy viscosity employed in this paper depends on the cutoff wavenumber k_c and the shape of the energy spectrum at the cutoff.

Models of κ_t are derived by similar arguments, i.e. by relating the turbulent

diffusivity to large-scale variables. Both models are then typically related via a turbulent Prandtl number Pr_t,

$$Pr_t = \nu_t/\kappa_t, \tag{1.9}$$

which is usually assumed to be constant. Its numerical value can in fact be derived by a direct application of the inertial-range velocity and scalar scaling laws of Kolmogorov and Obukhov–Corrsin. Let us now describe these scaling arguments.

We work in Fourier space and define the large-eddy filter by a sharp cutoff wavenumber k_c. The energy dissipation rate ϵ and the scalar dissipation rate χ are given by

$$\epsilon = 2\nu \int_0^\infty k^2 E(k)\,\mathrm{d}k, \qquad \chi = 2\kappa \int_0^\infty k^2 \Gamma(k)\,\mathrm{d}k,$$

where $E(k)$ is the energy spectrum of the turbulent velocity field and $\Gamma(k)$ is the scalar variance spectrum. Truncating the integrals and replacing the molecular viscosity and diffusivity by the turbulent viscosity and diffusivity to take into account the effect of all turbulent small scales below the grid (i.e. k above k_c) leads to

$$\epsilon \approx 2\nu_t \int_0^{k_c} k^2 E(k)\,\mathrm{d}k, \qquad \chi \approx 2\kappa_t \int_0^{k_c} k^2 \Gamma(k)\,\mathrm{d}k.$$

We assume that the cutoff k_c is within the inertial range of scales where

$$E(k) \approx C_K \epsilon^{2/3} k^{-5/3}, \qquad \Gamma(k) \approx C_{OC} \epsilon^{-1/3} \chi k^{-5/3},$$

where C_K is the Kolmogorov constant and C_{OC} is the Obukhov–Corrsin constant, and we find that

$$\nu_t \approx \tfrac{2}{3} C_K^{-3/2} \sqrt{\frac{E(k_c)}{k_c}}, \qquad \kappa_t \approx \tfrac{2}{3} C_K^{-1/2} C_{OC}^{-1} \sqrt{\frac{E(k_c)}{k_c}}.$$

It follows that

$$Pr_t = C_{OC}/C_K. \tag{1.10}$$

Leslie & Quarini (1979) were the first to suggest the energetic subgrid adjustment of the eddy viscosity; a more elaborate approach to eliminating the high-wavenumber part of the turbulence and incorporating its effect into an eddy viscosity was taken by Chollet & Lesieur (1981) who used a two-point closure theory (Kraichnan 1976) and obtained

$$\nu_t(k, k_c) = 0.267\, \nu^*(k/k_c) \left(\frac{E(k_c)}{k_c} \right)^{1/2} \tag{1.11}$$

where $\nu^*(k/k_c)$ is a non-dimensional eddy viscosity equal to 1 for $k \ll k_c$ with a sharp increase ('cusp') at $k \approx k_c$. The shape of ν^* has to be derived by the closure theory and an approximate fit is given by

$$\nu^*(x) = 1 + 34.49 \exp\left[-\frac{3.03}{x} \right]. \tag{1.12}$$

Chollet (1984) derived a similar model for the spectral eddy diffusivity

$$\kappa_t(k, k_c) = 0.445\, \kappa^*(k/k_c) \left(\frac{E(k_c)}{k_c} \right)^{1/2}. \tag{1.13}$$

However, additional free parameters in his two-point closure theory allow for a variety of different forms of $\kappa^*(k/k_c)$ and, as a consequence, Pr_t can be derived to be either

constant and equal to 0.6 even in the vicinity of k_c, or equal to the constant value 0.33 for $k \ll k_c$ with a sharp increase just before k_c leading to a peak value of 0.6 at the cusp.

In any case, the constant numerical value of Pr_t is based on the assumption of inertial-range scaling for both the velocity and scalar fields, and should be $Pr_t \approx 0.6$ for consistency. However, whereas a well-defined Kolmogorov inertial-range scaling $E(k) = C_K \epsilon^{2/3} k^{-5/3}$ has been observed in many high-Reynolds-number flows (Sreenivasan 1995), no such unqualified evidence exists for the corresponding Obukhov–Corrsin scalar inertial range $\Gamma(k) = C_{OC} \epsilon^{-1/3} \chi k^{-5/3}$. For example, the issue of the universality of the constant C_{OC} is still debated (see, for example, Sreenivasan 1996); this discussion may be linked to the issue of the different values of Pr_t used in LES of different flows. Also, in the case of finite Reynolds numbers, the spectral exponents p and q of the velocity power spectra $E(k) \sim k^{-p}$ and the scalar variance spectra $\Gamma(k) \sim k^{-q}$ frequently show different behaviour with $p, q \leqslant \frac{5}{3}$ and $p > q$ both in experiments (Mydlarski & Warhaft 1998) and in direct numerical simulations (Pumir 1994). Finally, in an isotropic LES of a passive scalar field by Lesieur & Rogallo (1989) (with eddy viscosity ν_t and eddy diffusivity κ_t both obtained under the assumption of universality and inertial-range exponents $p = q = \frac{5}{3}$) the passive scalar field showed an anomalous scaling behaviour $\Gamma(k) \sim k^{-1}$ in the inertial–convective range of scales which is inconsistent with the underlying modelling assumptions. In fact, it is well-known that even in DNS with passive scalar fields where $Pr = O(1)$ the intensity of fluctuations in the scalar small scales seems to be much more pronounced than in the velocity field (Pumir 1994; Bogucki, Domaradzki & Yeung 1997). None of these different pieces of evidence support the idea that Pr_t is a universal constant.

1.3. *Kinematic simulation and small-scale turbulent flow structure*

In this work we propose to use pairs of fluid elements to describe passive scalar fluctuations, which entails advecting ideal particles through a large-eddy simulated velocity field. The turbulent Lagrangian velocity of these particles results from the large-eddy field (which is known) plus the contribution from the small-scale subgrid field (which is not known). The mean scalar field is dominated by the turbulent large scales and we may therefore expect that particles advected by the large-eddy field only (plus perhaps some additional randomness to correct for the turbulent kinetic energy which is contained in the small scales) is a good approximation of the mean scalar field. However, here we are interested in simulating concentration variances which are determined by all turbulent scales, including in particular the small scales which are not explicitly computed but filtered out.

Can we find an explicit form of the subgrid velocity field which incorporates the effects of the small-scale turbulence flow structure on Lagrangian relative statistics sufficiently accurately and which is compatible with and can be consistently superimposed on the supergrid velocity field? This means in particular that the modelled subgrid velocity field should be incompressible, obey Kolmogorov's inertial-range scaling properties, and contain the vortical, straining and streaming regions that exist in the small scales of the turbulence.

Lagrangian stochastic models define the stochastic velocities only in a Lagrangian frame whereas every flow realization of a kinematic simulation is based on an incompressible Eulerian flow field with eddying, straining and streaming regions (Fung *et al.* 1992; Fung & Vassilicos 1998). Indeed, kinematic simulations are non-Markovian Lagrangian models where it is the eddying, straining and other structures that account for the statistical properties of the velocity field but it is the straining

structures that are mostly responsible for particles moving apart from each other (Fung *et al.* 1992; Fung & Vassilicos 1998).

An appropriate model for a subgrid advection velocity of the fluid elements should not only reproduce the correct scaling properties but also correct absolute values. The absolute value of particle-pair separation is determined by the dimensionless Richardson constant G_Δ. The only experimental measurement of G_Δ known to the present authors is that of Tatarski (1960) who obtained $G_\Delta = 0.06$. Unfortunately, his measurements are fraught with uncertainty but one can perhaps say, with some confidence, that G_Δ is a number between $O(10^{-2})$ and $O(10^{-1})$. Turbulence closures such as LHDIA and EDQNM lead to much larger values of G_Δ in the range 2.42 to 3.5; and stochastic models (e.g. Thomson 1990) also give $G_\Delta = O(10^{-1})$. However, kinematic simulations of turbulent-like velocity fields yield $G_\Delta = O(10^{-2})$ to $O(10^{-1})$ and thus support the experimental data of Tatarski (1960) (see also Fung *et al.* 1992; Elliott & Majda 1996 and Fung & Vassilicos 1998 for a discussion on the value of G_Δ). This may not come as a surprise because it is now well established that persisting flow structures exist in the turbulent small scales (Jiménez & Wray 1998 and references therein; Cadot, Douady & Couder 1995), and such long-lived spatial flow structure does not seem to be currently well incorporated in stochastic models. The point that we make is that spatio-temporal flow structure strongly influences two-particle statistics. On the other hand, one-particle statistics are not so significantly affected by flow structure, which is consistent with the ability of even random walk models to correctly represent average scalar statistics.

The importance of small-scale turbulent flow structure has been also emphasized by Malik & Vassilicos (1999) who studied (among other statistics) the Lagrangian two-particle relative velocity flatness which is a measure of the velocity field's intermittency. Their results agree well with DNS predictions (Yeung 1994) and show much higher flatnesses than stochastic models (Heppe 1998). The difference has been explained by the qualitative difference of the velocities that are generated by KS and current stochastic models, respectively.

Another important difference (besides the incorporation of flow structure) between stochastic models and kinematic simulations is that the Lagrangian integral time scale T_L is a model input parameter of the stochastic model whereas it is an output of kinematic simulations. For a stochastic model this parameter is a function of the Lagrangian inertial-range constant C_0 which is usually chosen such that it corresponds to Lagrangian experimental data ($C_0 \approx 4$). These data are however highly uncertain, and stochastic model simulations have been reported where C_0 has been simply chosen such as to fit experimental scalar variance results (see, for example, Borgas & Sawford 1996). The same authors in fact propose to use a C_0 much in excess of the experimentally suggested value, i.e. $C_0 > 6$, for a better fit with the corresponding variance statistics.

1.4. *Plan of the paper*

The plan of the paper is as follows. In § 2 we give some background on the way that fluid element statistics are related to the scalar field's statistics. In § 3 we describe kinematic simulation in some detail and investigate its performance as a Lagrangian model of particle dispersion. In § 4 we present the kinematic subgrid model. We demonstrate how the kinematic model flow can be used in simulating scalar dispersion with explicitly resolving inertial-range scaling and flow structure effects. We discuss the effect of the inertial-range velocity field on two-particle probability densities and discuss the results obtained for the release from an instantaneous line source. In

particular, we discuss the effect that the small value of G_Δ has on scalar variance statistics. Finally, we conclude in § 5.

2. Fluid element concentration statistics

In this section we state the theoretical results concerning the relation between particle and scalar statistics that we need to use in our LES-KS modelling. For more detailed information on fluid element statistics the reader is referred, for example, to Thomson (1990). We also introduce Sawford's (1983) approximation which is useful (if not essential) to compute scalar variances numerically.

2.1. *The separation p.d.f.*

The first and second moments of the scalar concentration are related to the statistics of the motion of single particles and particle pairs, respectively. Relations between higher-order moments and multiple particle statistics can also be derived formally (Egbert & Baker 1984). This section is devoted to first- and second-order moments and we introduce the appropriate approximations to make the concentration variance field accessible to computations based on clouds of particles.

Neglecting effects of molecular diffusion, the mean concentration field $\langle\theta(\boldsymbol{x},t)\rangle$ is generally the weighted sum of concentrations assigned to single particles at their release from points $\boldsymbol{x}'$ at times t' reaching the observation point $\boldsymbol{x}$ at time t:

$$\langle\theta(\boldsymbol{x},t)\rangle = \int_{t'<t}\int P_1(\boldsymbol{x},t;\boldsymbol{x}',t')S(\boldsymbol{x}',t')\,\mathrm{d}\boldsymbol{x}'\,\mathrm{d}t', \tag{2.1}$$

where P_1 is the probability density function (p.d.f.) for a particle which is at $\boldsymbol{x}$ at time t to have come from $\boldsymbol{x}'$ at a time t' prior to t ($t'<t$). The brackets $\langle\cdot\rangle$ denote ensemble averages. Similarly, the two-point correlation is given by

$$\begin{aligned}\langle\theta(\boldsymbol{x}_1,t)\theta(\boldsymbol{x}_2,t)\rangle = {} & \int\int_{t_1',t_2'<t}\int\int P_2(\boldsymbol{x}_1,\boldsymbol{x}_2,t;\boldsymbol{x}_1',\boldsymbol{x}_2',t_1',t_2')S(\boldsymbol{x}_1',t_1')\\ & \times S(\boldsymbol{x}_2',t_2')\,\mathrm{d}\boldsymbol{x}_1'\,\mathrm{d}\boldsymbol{x}_2'\,\mathrm{d}t_1'\,\mathrm{d}t_2'\end{aligned} \tag{2.2}$$

where P_2 is the p.d.f. for two particles which are at $\boldsymbol{x}_1$ and $\boldsymbol{x}_2$ at time t to have come from $\boldsymbol{x}_1'$ and $\boldsymbol{x}_2'$ at times t_1', t_2' prior to t ($t_1', t_2' < t$). Equations (2.1) and (2.2) are valid for arbitrary source distributions in space and time.

Here we restrict ourselves to instantaneous source releases so that $S(\boldsymbol{x}',t') = S(\boldsymbol{x}')\delta(t'-t_0)$ where δ is the delta function and t_0 is the time of instantaneous release. In the case of non-instantaneous releases, the particle ensemble that is necessary to obtain a converged P_2 numerically can be prohibitively large, but also theoretical studies to date (see, for example, Thomson 1996) mainly address instantaneous releases. Note however that an instantaneous release from a line or area source in stationary, isotropic turbulence is a good approximation of a continuous release from a point or line source, respectively, in stationary turbulence with a constant mean wind (Sawford 1983).

For an instantaneous release, (2.1) and (2.2) become

$$\langle\theta(\boldsymbol{x},t)\rangle = \int P_1(\boldsymbol{x},t;\boldsymbol{x}',t_0)S(\boldsymbol{x}')\,\mathrm{d}\boldsymbol{x}', \tag{2.3}$$

$$\langle\theta(\boldsymbol{x}_1,t)\theta(\boldsymbol{x}_2,t)\rangle = \int\int P_2(\boldsymbol{x}_1,\boldsymbol{x}_2,t;\boldsymbol{x}_1',\boldsymbol{x}_2',t_0)S(\boldsymbol{x}_1')S(\boldsymbol{x}_2')\,\mathrm{d}\boldsymbol{x}_1'\,\mathrm{d}\boldsymbol{x}_2'. \tag{2.4}$$

We are particularly interested in the concentration variance field $\langle\theta^2(\boldsymbol{x},t)\rangle$. To take into account the effect of molecular diffusion, Durbin (1980) averages over a sphere of diameter equal to one appropriate dissipative microscale η (which is much smaller than the integral length scale L of the turbulence). The limit $|\boldsymbol{x}_1-\boldsymbol{x}_2|/L\to 0$, which is different from $|\boldsymbol{x}_1-\boldsymbol{x}_2|/\eta\to 0$, is approximately equal to the average over the volume V_η ($\sim O(\eta^3)$) of this sphere centred at $\boldsymbol{x}$, i.e.

$$\begin{aligned} p_2(\boldsymbol{x},t;\boldsymbol{x}_1',\boldsymbol{x}_2',t_0) &\equiv \frac{1}{V_\eta}\int_{V_\eta}\frac{1}{V_\eta}\int_{V_\eta} P_2(\boldsymbol{x}_1,\boldsymbol{x}_2,t;\boldsymbol{x}_1',\boldsymbol{x}_2',t_0)\,\mathrm{d}\boldsymbol{x}_1\,\mathrm{d}\boldsymbol{x}_2 \\ &\approx \lim_{\substack{|\boldsymbol{x}-\boldsymbol{x}_1|/L\to 0\\ |\boldsymbol{x}-\boldsymbol{x}_2|/L\to 0}} P_2(\boldsymbol{x}_1,\boldsymbol{x}_2,t;\boldsymbol{x}_1',\boldsymbol{x}_2',t_0). \end{aligned} \tag{2.5}$$

This limit effectively means that $|\boldsymbol{x}_1-\boldsymbol{x}_2|/\eta$ is of order one in the limit of high Reynolds numbers where $L/\eta\to\infty$. The microscale η may be unambiguously identified with the Kolmogorov scale η_K when $Pr=\nu/\kappa=O(1)$. Durbin (1980) then computes $\langle\theta^2(\boldsymbol{x},t)\rangle$ by using (2.4) and (2.5) as follows:

$$\begin{aligned} \langle\theta(\boldsymbol{x},t)^2\rangle &= \frac{1}{V_\eta}\int_{V_\eta}\frac{1}{V_\eta}\int_{V_\eta}\langle\theta(\boldsymbol{x}_1,t)\theta(\boldsymbol{x}_2,t)\rangle\,\mathrm{d}\boldsymbol{x}_1\,\mathrm{d}\boldsymbol{x}_2 \\ &= \int\int p_2(\boldsymbol{x},t;\boldsymbol{x}_1',\boldsymbol{x}_2',t_0)S(\boldsymbol{x}_1')S(\boldsymbol{x}_2')\,\mathrm{d}\boldsymbol{x}_1'\,\mathrm{d}\boldsymbol{x}_2'. \end{aligned} \tag{2.6}$$

Equation (2.6) is important in this study as it transforms the problem of calculating the concentration variance into one of determining the two-particle p.d.f. p_2 (assuming, of course, that the source distribution is known). We now discuss the assumptions and method for calculating this p.d.f.

2.2. *Computing the separation p.d.f.*

Sawford's working assumptions

To determine P_2 and therefore p_2 numerically is computationally very expensive because it requires a large number of particles. Sawford (1983) introduced a very useful approximation to reduce the numerical cost and we will make use of this approximation. We note first that particle pairs can be equivalently described either by the particle positions $\boldsymbol{x}_1,\boldsymbol{x}_2$ or by the relative separation $\boldsymbol{\Delta}$ and the centre of mass $\boldsymbol{z}$:

$$\boldsymbol{\Delta}=\boldsymbol{x}_1-\boldsymbol{x}_2,\quad \boldsymbol{z}=\boldsymbol{x}_1+\boldsymbol{x}_2,$$

$$P_2(\boldsymbol{\Delta},\boldsymbol{z},t;\boldsymbol{\Delta}',\boldsymbol{z}',t_0)\,\mathrm{d}\boldsymbol{\Delta}'\,\mathrm{d}\boldsymbol{z}'=P_2(\boldsymbol{x}_1,\boldsymbol{x}_2,t;\boldsymbol{x}_1',\boldsymbol{x}_2',t_0)\,\mathrm{d}\boldsymbol{x}_1'\,\mathrm{d}\boldsymbol{x}_2'.$$

For Durbin's limit where $|\boldsymbol{x}_1-\boldsymbol{x}_2|/L\to 0$ we write

$$P_2(\boldsymbol{\Delta}_0,\boldsymbol{z},t;\boldsymbol{\Delta}',\boldsymbol{z}',t_0)\,\mathrm{d}\boldsymbol{\Delta}'\,\mathrm{d}\boldsymbol{z}'=\lim_{\substack{|\boldsymbol{x}-\boldsymbol{x}_1|/L\to 0\\ |\boldsymbol{x}-\boldsymbol{x}_2|/L\to 0}} P_2(\boldsymbol{x}_1,\boldsymbol{x}_2,t;\boldsymbol{x}_1',\boldsymbol{x}_2',t_0)\,\mathrm{d}\boldsymbol{x}_1'\,\mathrm{d}\boldsymbol{x}_2', \tag{2.7}$$

where $|\boldsymbol{\Delta}_0|=O(\eta)$ and $\boldsymbol{z}=2\boldsymbol{x}$. Note that P_2 may be assumed to be a function of $|\boldsymbol{\Delta}_0|$ only rather than $\boldsymbol{\Delta}_0$ because of the isotropizing effect of molecular diffusion at scales of the order of η and below. Except where stated otherwise, in this paper's numerical simulations we set $|\boldsymbol{\Delta}_0|=\eta$ (which is equal to η_K because we restrict ourselves to flows where $Pr\sim O(1)$). From (2.5) and (2.7)

$$P_2(\boldsymbol{\Delta}_0,\boldsymbol{z},t;\boldsymbol{\Delta}',\boldsymbol{z}',t_0)\,\mathrm{d}\boldsymbol{\Delta}'\,\mathrm{d}\boldsymbol{z}'\approx p_2(\boldsymbol{x},t;\boldsymbol{x}_1',\boldsymbol{x}_2',t_0)\,\mathrm{d}\boldsymbol{x}_1'\,\mathrm{d}\boldsymbol{x}_2', \tag{2.8}$$

where $|\Delta_0| = O(\eta)$ and $z \approx 2x$. Equation (2.8) relates the two-particle p.d.f. p_2 in (2.6) to the p.d.f. $P_2(\Delta_0, z, t; \Delta', z', t_0)$ of relative separations and centres of mass. Sawford's assumptions concern this p.d.f. $P_2(\Delta_0, z, t; \Delta', z', t_0)$.

Sawford's first assumption is one of statistical independence of Δ and z, i.e.

$$P_2(\Delta_0, z, t; \Delta', z', t_0) \approx p_\Delta(\Delta_0, t; \Delta', t_0) p_z(z, t; z', t_0). \tag{2.9}$$

It is not clear how appropriate this assumption is in general, but it is routinely used in stochastic models and we use it here too. In stochastic models Δ and z are by construction statistically uncorrelated for all times. In §4.4 we validate this assumption of independence for our modelling approach.

Sawford's second assumption is that x and z are both normally distributed. And his third assumption is that the instantaneous source is a Gaussian. Denoting a d-dimensional Gaussian distribution of variance σ^2 by G_d, that is

$$G_d(x, \sigma^2) = \begin{cases} \dfrac{1}{(2\pi)^{3/2}\sigma^3} \exp\left[-|x|^2/2\sigma^2\right], & d = 3 \\ \dfrac{1}{2\pi\sigma^2} \exp\left[-(y^2 + z^2)/2\sigma^2\right], & d = 2 \\ \dfrac{1}{(2\pi)^{1/2}\sigma} \exp\left[-z^2/2\sigma^2\right], & d = 1, \end{cases} \tag{2.10}$$

these two assumptions can be specified as

$$\left.\begin{aligned} P_1(x, t; x', t_0) &\approx G_3(x' - x, \sigma_x^2(t_0; t)), \\ p_z(z, t; z', t_0) &\approx G_3(z' - z, \sigma_z^2(t_0; t)) \end{aligned}\right\} \tag{2.11}$$

for the p.d.f.s of single particles and centres of mass of particle pairs, and

$$S(x) = G_d(x, \sigma_0^2) \tag{2.12}$$

for the instantaneous source distribution, according to whether the source is a point source ($d = 3$), a line source ($d = 2$) or a plane area source ($d = 1$). The variances σ_x^2 and σ_z^2 are, respectively, those of x and z at a time t following release at a time t_0. And σ_0^2 in (2.12) is the variance of the Gaussian source and may be interpreted as a measure of the size of the actual source.

Thus, using (2.11) and (2.12) in (2.3) the mean concentration field is Gaussian

$$\langle \theta(x, t) \rangle = G_d(x, \sigma_0^2 + \sigma_x(t_0; t)^2), \tag{2.13}$$

which is generally well accepted as a good approximation for the mean concentration field (Sawford 1983). Using (2.11), (2.12) and (2.9) in (2.6) the mean variance field is

$$\langle \theta^2(x, t) \rangle = \left[\int p_\Delta(\Delta_0, t; \Delta', t_0) G_d(\Delta', \sigma_0^2)\, \mathrm{d}\Delta' \right] G_d(2x, \sigma_z(t_0; t)^2 + \sigma_0^2) \tag{2.14}$$

with $|\Delta_0| = \eta$. Equation (2.14) is of crucial importance to this study because it reduces the calculation of $\langle \theta^2(x, t) \rangle$ to the computation of $p_\Delta(\Delta_0, t; \Delta', t_0)$ and $\sigma_z(t_0; t)$. Whilst the calculation of $\sigma_z(t_0; t)$ is straightforward, that of $p_\Delta(\Delta_0, t; \Delta', t_0)$ for a fixed $|\Delta_0|$ is not, and we attempt to reduce its calculation to the much easier calculation of $p_\Delta(\Delta', t; \Delta_0, t_0)$ for a fixed $|\Delta_0|$.

Backward versus forward diffusion

The numerical computation of $p_\Delta(\Delta_0, t; \Delta', t_0)$ for a fixed $|\Delta_0|$ is very impractical because it requires integrating pairs of trajectories for all possible initial (t_0) separations

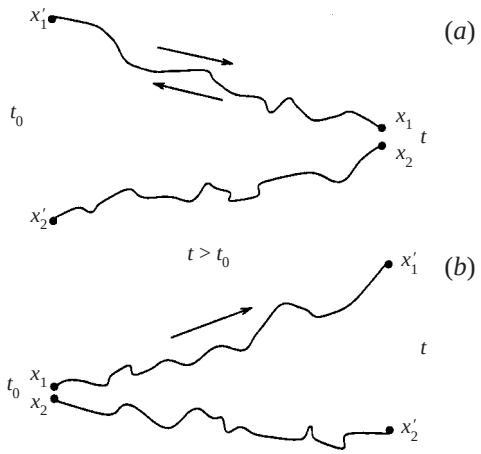

FIGURE 1. Time reversal for the movements of particle pairs. (*a*) There is no difference for particles starting from $\boldsymbol{x}_1', \boldsymbol{x}_2', t_0$ and arriving at $\boldsymbol{x}_1, \boldsymbol{x}_2, t$ (moving forwards in time); and particles starting from $\boldsymbol{x}_1, \boldsymbol{x}_2, t$ and arriving at $\boldsymbol{x}_1', \boldsymbol{x}_2', t_0$ (moving backwards in time). (*b*) However, particles starting at $\boldsymbol{x}_1, \boldsymbol{x}_2, t_0$ and arriving at $\boldsymbol{x}_1', \boldsymbol{x}_2', t$ may *a priori* not be expected to have the same statistics.

$\boldsymbol{\Delta}'$ and keeping only the tiny fraction of those pairs which, at time t, are at a distance $|\boldsymbol{\Delta}_0|$ from each other. However, in Monte Carlo simulations of stochastic models (e.g. Thomson 1990) it is common to use a symmetry property of P_1 and P_2 (Egbert & Baker 1984), namely (see figure 1*a*)

$$\left.\begin{aligned} &P_1(\boldsymbol{x}, t; \boldsymbol{x}', t_0) = P_1(\boldsymbol{x}', t_0; \boldsymbol{x}, t), \\ &P_2(\boldsymbol{x}_1, \boldsymbol{x}_2, t; \boldsymbol{x}_1', \boldsymbol{x}_2', t_0) = P_2(\boldsymbol{x}_1', \boldsymbol{x}_2', t_0; \boldsymbol{x}_1, \boldsymbol{x}_2, t), \end{aligned}\right\} \tag{2.15}$$

which implies when (2.9) is valid and because $p_z(\boldsymbol{z}, t; \boldsymbol{z}', t_0) = p_z(\boldsymbol{z}', t_0; \boldsymbol{z}, t)$, that

$$p_{\Delta}(\boldsymbol{\Delta}_0, t; \boldsymbol{\Delta}', t_0) = p_{\Delta}(\boldsymbol{\Delta}', t_0; \boldsymbol{\Delta}_0, t). \tag{2.16}$$

Hence, it is possible to calculate $p_{\Delta}(\boldsymbol{\Delta}_0, t; \boldsymbol{\Delta}', t_0)$ by integrating pairs of trajectories backwards in time starting at time t with separation $\boldsymbol{\Delta}_0$ and recording all separations $\boldsymbol{\Delta}'$ at time $t_0 < t$. Such a scheme is clearly more practical than the direct calculation of $p_{\Delta}(\boldsymbol{\Delta}_0, t; \boldsymbol{\Delta}', t_0)$ described above but requires an integration backwards in time.

Unfortunately the particles in the present study are advected by Navier–Stokes dynamics which do not possess time-reversal symmetry and therefore cannot be integrated backwards in time. It is not clear how, in general, the backward diffusion p.d.f. $p_{\Delta}(\boldsymbol{\Delta}', t_0; \boldsymbol{\Delta}_0, t)$ and the forward diffusion p.d.f. $p_{\Delta}(\boldsymbol{\Delta}', t; \boldsymbol{\Delta}_0, t_0)$ differ quantitatively (see figure 1). However, in stationary turbulence the backward and forward diffusion p.d.f.s are equivalent (Sawford & Hunt 1986) and we can integrate forwards in time to calculate $p_{\Delta}(\boldsymbol{\Delta}', t; \boldsymbol{\Delta}_0, t_0)$ for a fixed $|\boldsymbol{\Delta}_0|$ as a proxy for $p_{\Delta}(\boldsymbol{\Delta}_0, t; \boldsymbol{\Delta}', t_0)$. We note, however, that the validity of using $p_{\Delta}(\boldsymbol{\Delta}', t; \boldsymbol{\Delta}_0, t_0)$ has to be checked in non-stationary flow configurations.

The separation p.d.f. in isotropic flows

We remark that $p_{\Delta}(\boldsymbol{\Delta}_0, t; \boldsymbol{\Delta}', t_0)$ in (2.14) as well as the forward diffusion p.d.f. $p_{\Delta}(\boldsymbol{\Delta}', t; \boldsymbol{\Delta}_0, t_0)$ are p.d.f.s of the three-dimensional vectors $\boldsymbol{\Delta}_0$ and $\boldsymbol{\Delta}'$. Both these p.d.f.s are numerically very costly to compute and it is useful to take advantage of the symmetries of p_{Δ}. In what follows we concentrate on $p_{\Delta}(\boldsymbol{\Delta}', t; \boldsymbol{\Delta}_0, t_0)$ but these

simplifications can be introduced for the backward p.d.f. $p_\Delta(\boldsymbol{\Delta}_0, t; \boldsymbol{\Delta}', t_0)$ in a similar way.

In an isotropic flow $p_\Delta(\boldsymbol{\Delta}', t; \boldsymbol{\Delta}_0, t_0)$ is a function of $\Delta_0 = |\boldsymbol{\Delta}_0|$ and $\Delta' = |\boldsymbol{\Delta}'|$ only, i.e.

$$p_\Delta(\boldsymbol{\Delta}', t; \boldsymbol{\Delta}_0, t_0) = p_\Delta(\Delta', t; \Delta_0, t_0). \tag{2.17}$$

The right-hand side is equivalent to the one-dimensional p.d.f.

$$p_\Delta(\Delta', t; \Delta_0, t_0) = p_\Delta(\Delta'_x, t; \Delta_0, t_0 \mid \Delta'_y = 0 \text{ and } \Delta'_z = 0) \tag{2.18}$$

provided that the p.d.f. on the right-hand side is computed by choosing initial particle separations Δ_0 at time t_0 which are randomly and isotropically distributed; at time t one then computes $\Delta'_x = i\, d\Delta'_x$ with $i = 0 \ldots N$ by using a limited number N of increments $d\Delta'_x$ for all $\Delta'_y, \Delta'_z \in [0, d\Delta'_x]$. Likewise, we can define a one-dimensional p.d.f. where averages are performed either on one other component or on two components of $\boldsymbol{\Delta}'$:

$$\left.\begin{aligned} &\overline{p}_\Delta(\Delta'_x, t; \Delta_0, t_0 \mid \Delta'_y = 0 \text{ or } \Delta'_z = 0), \\ &\overline{\overline{p}}_\Delta(\Delta'_x, t; \Delta_0, t_0). \end{aligned}\right\} \tag{2.19}$$

$\overline{p}_\Delta$ is useful for computing variances from a line source (where averages are performed along the source distribution); and similarly, $\overline{\overline{p}}_\Delta$ is useful for computing variances from an area source. In § 4.4 we compute the p.d.f.s p_Δ, $\overline{p}_\Delta$ and $\overline{\overline{p}}_\Delta$ to identify inertial-range effects on these p.d.f.s and, in particular, we use $\overline{p}_\Delta$ to compute the scalar variance from a line source where we can compare our model with experimental results.

3. Two-particle dispersion in three-dimensional kinematic simulations

3.1. *Kinematic simulations*

Following Kraichnan (1970), Drummond, Duane & Horgan (1984) and Fung *et al.* (1992) 'kinematic simulations' of turbulence are based on random flow fields (as opposed to simulation techniques based on dynamical equations of motion) that obey incompressibility and certain statistical properties that are known from theory and experiments. The random flow fields provided by kinematic simulations are presented here with a view of using them as a means to incorporate the effect of the turbulent small scales on the scalar field. This implies that the random flow field has to follow Kolmogorov's inertial-range scaling. The numerical procedure to create such fields is as follows.

Similarly to Fung *et al.* (1992) and Malik & Vassilicos (1999) we generate an incompressible three-dimensional turbulent-like velocity field $\boldsymbol{u}_{KS}(\boldsymbol{x}, t)$ by summing different Fourier modes

$$\boldsymbol{u}_{KS}(\boldsymbol{x}, t) = \sum_{n=1}^{N_k} \left(\boldsymbol{a}_n \cos\left(\boldsymbol{k}_n \boldsymbol{x} + \omega_n t\right) + \boldsymbol{b}_n \sin\left(\boldsymbol{k}\boldsymbol{x} + \omega_n t\right)\right), \tag{3.1}$$

where N_k is the number of Fourier modes, $\boldsymbol{a}_n$ and $\boldsymbol{b}_n$ are the amplitudes corresponding to wavevector $\boldsymbol{k}_n$, and ω_n is an unsteadiness frequency. Such velocity fields have been shown to be stationary in time and space (Fung *et al.* 1992; Fung & Vassilicos 1998). The wavevectors $\boldsymbol{k}_n$ are randomly distributed in spherical shells,

$$\boldsymbol{k}_n = k_n(\sin\theta\cos\phi, \sin\theta\sin\phi, \cos\theta)$$

with uniformly distributed random angles $\theta \in [0, 2\pi]$, $\phi \in [0, \pi]$. The amplitudes $\boldsymbol{a}_n$,

$\boldsymbol{b}_n$ are random uncorrelated vectors such that

$$\boldsymbol{a}_n \boldsymbol{k}_n = \boldsymbol{b}_n \boldsymbol{k}_n = 0$$

to ensure incompressibility, and

$$|\boldsymbol{a}_n|^2 = |\boldsymbol{b}_n|^2 = 2E(k_n)\Delta k_n,$$

where $E(k)$ is a prescribed Eulerian self-similar energy spectrum of the form

$$E(k) = \begin{cases} C_K \epsilon^{2/3} k^{-5/3} & \text{for } k_1 < k < k_\eta \\ 0 & \text{otherwise.} \end{cases} \tag{3.2}$$

C_K is the Kolmogorov dimensionless constant (and we choose $C_K = 1.5$ throughout this study in agreement with reference data, e.g. Sreenivasan 1995), ϵ is a constant with dimensions of a dissipation rate, and k_1, k_η (with $\eta = 2\pi/k_\eta$) define the range of wavenumbers where the random velocity field obeys the $-\frac{5}{3}$ inertial-range scaling law. A variety of different distributions of modes k_n may be used and following Fung *et al.* (1992) we choose among algebraic, geometric and linear distributions,

$$k_n = \begin{cases} k_1 \left(\dfrac{k_\eta}{k_1}\right)^{n-1/N_k-1} & \text{(geometric)} \\ k_1 n^{\log(k_\eta/k_1)/\log N_k} & \text{(algebraic)} \\ k_1 + \left(\dfrac{k_\eta - k_1}{N_k - 1}\right)(n-1) & \text{(linear),} \end{cases} \tag{3.3}$$

with $n \in [1, N_k]$, $\Delta k_n = (k_{n+1} - k_{n-1})/2$ for $n \in [2, N_k - 1]$, and $\Delta k_1 = (k_2 - k_1)/2$, $\Delta k_{N_k} = (k_{N_k} - k_{N_k-1})/2$.

The unsteadiness frequency ω_n can be chosen at will and it has been proposed that $\omega_n \sim \sqrt{k_n^3 E(k_n)}$, i.e. ω_n is proportional to the eddy-turnover time of wavemode n (Fung *et al.* 1992; Fung & Vassilicos 1998); or that $\omega_n \sim U k_n$, i.e. all modes are advected with a constant velocity U (Turfus & Hunt 1987; Elliott & Majda 1996). Previous studies of three-dimensional KS fields suggest that the choice of ω_n has no significant influence on most statistical properties of particle pairs for times t smaller than the integral time scale T_L, and as long as $\omega_n/\sqrt{k_n^3 E(k_n)}$ or $\omega_n/(U k_n)$ are not much larger than 1 (Malik 1996; Malik & Vassilicos 1999). In preliminary simulations for the present study we have confirmed this observation on the r.m.s. of particle-pair separations $\sqrt{\langle \Delta^2 \rangle}$, and have therefore set $\omega_n = 0$ for all n in the remainder of this paper. We suspect that this insensitivity to ω_n is characteristic of three-dimensional turbulent-like flows where, unlike two-dimensional flows, streamlines can have a chaotic structure (Ottino 1989).

We stress that there are no free parameters in this simulation technique (of course, the shape of the energy spectrum could, at least in principle, be viewed as a free parameter); the number of modes N_k and the mode distribution are chosen such that the resulting statistics converge. We also stress that the KS flow field (3.1) is not a model of Eulerian turbulence, but the basis for a Lagrangian model of turbulent dispersion. Malik & Vassilicos (1999) have demonstrated the very good agreement between KS and DNS Lagrangian two-particle statistics for numbers of KS modes N_k as small as about 100!

Despite the simplicity of the method, the numerical cost of performing the sum in (3.1) can be very large for an order of 100 Fourier modes because FFTs cannot be used in KS. Therefore, we adopt the adaptive time-stepping procedure proposed by Elliott & Majda (1996) to compute two-particle statistics over a large range of times.

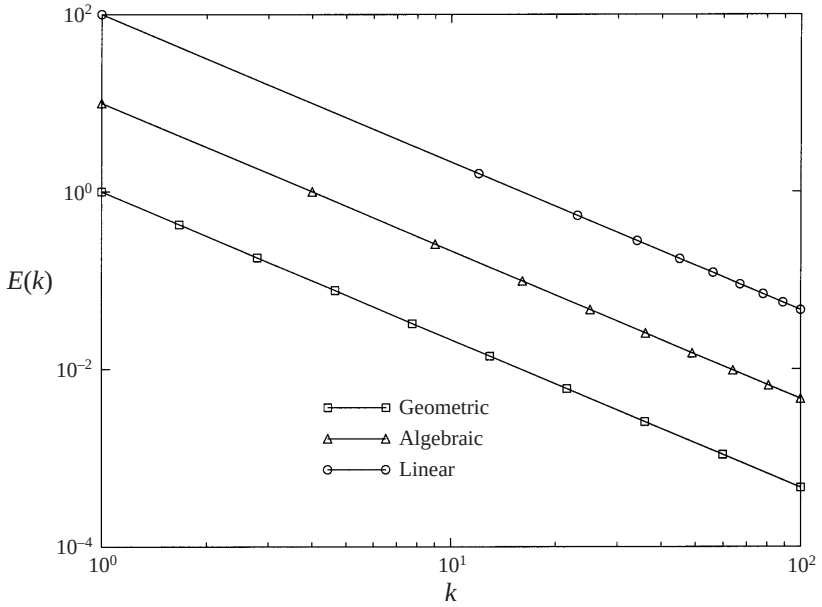

FIGURE 2. Log-log plot of the energy spectrum (3.2) for $N_k = 10$ modes and different mode distributions (3.3). The symbols indicate the values of the k_n and the geometric distribution leads to equally spaced energy shells for $\log(k)$, the linear distribution has most wavenumbers packed in the highest modes, and the algebraic distribution is somewhere in between.

Assuming that the separation statistics are determined by eddies of size $\sqrt{\langle \Delta^2 \rangle}$ only (this is essentially the locality assumption, for more details see Fung & Vassilicos 1998), Elliott & Majda (1996) propose to use an adaptive time step $\mathrm{d}t_a$ given by

$$\mathrm{d}t_a = \alpha \sqrt{\langle \Delta^2(t) \rangle} \left| \frac{\mathrm{d}\sqrt{\langle \Delta^2(t) \rangle}}{\mathrm{d}t} \right|^{-1} \tag{3.4}$$

with a constant $\alpha < 1$. We set $\alpha = 0.25$ for all simulations presented here but found no changes in particle-pair statistics for other values of α. We tested the adaptive time-stepping procedure by comparing it to a few (very time consuming) simulations with constant time stepping; no significant difference in the two-particle statistics was observed between adaptive and constant time steps.

In figure 2 we plot the energy spectrum (3.2) for $N_k = 10$ modes and different wavenumber distributions, (3.3). It is shown that the geometric distribution leads to equally spaced energy shells for $\log(k)$ whereas the linear distribution has most wavenumbers packed in the highest modes. The algebraic distribution is somewhere in between. We investigated which of these distributions leads to the fastest converging statistics. In figure 3 we plot the Lagrangian velocity correlation function for the different mode distributions and for different numbers of Fourier modes. The distributions converge towards an exponential decay $\exp(-t/T_L)$ where $T_L = 0.65$. It is also seen that the geometric distribution leads to the fastest convergence; no significant difference is seen for the cases $N_k = 20$ and $N_k = 200$. This may not be too surprising because, for the same N_k, the geometric distribution has more modes than the other distributions in the low wavenumbers which dominate the correlation function. For the algebraic and linear distributions the correlation function is still far from converged when $N_k = 20$. We also compared the mean separation of par-

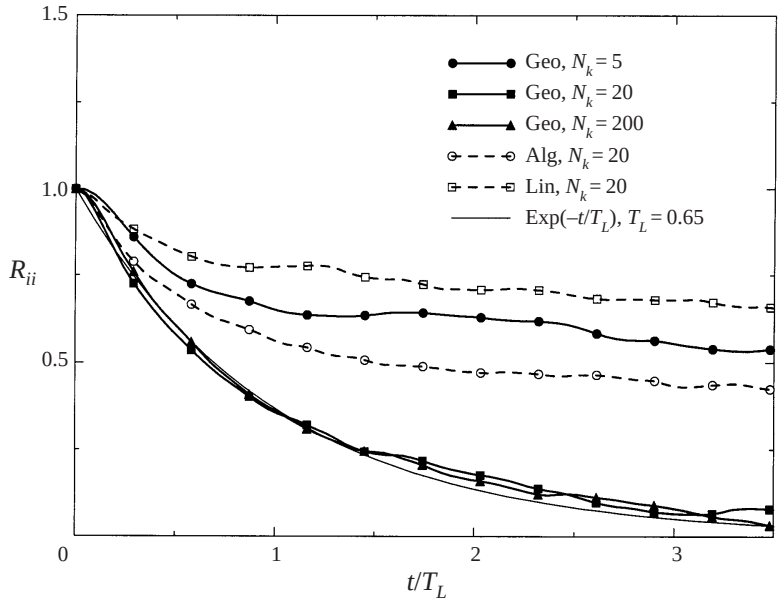

FIGURE 3. The effect of different mode distributions on the Lagrangian velocity correlation function $R_{ii} = \langle u_i(t_0)u_i(t_0+t)\rangle/\langle u_i^2\rangle$, where u_i are the components of the Lagrangian turbulent velocity. The distributions converge towards an exponential decay $\exp(-t/T_L)$ where $T_L = 0.65$. The geometric distribution leads to fastest convergence in terms of the number of modes needed.

ticles for different distributions and found no significant differences. This was to be expected because the turbulent small scales dominate the two-particle statistics, and the difference between the mode distributions is not so marked at the small scales. As a consequence, all the results presented in the rest of this paper are obtained using the geometric distribution of wavenumbers.

3.2. *Two-particle dispersion*

In this section we investigate the performance of KS with respect to two-particle statistics. Previous studies of two-particle statistics which were obtained from KS showed either only very short ranges of inertial scaling in three dimensions (Fung *et al.* 1992) or were restricted to two dimensions (Elliott & Majda 1996; Fung & Vassilicos 1998). By applying Elliott & Majda's (1996) time-stepping procedure to the three-dimensional KS velocity field (3.1) we are able to obtain a scaling range that is significantly larger than that of Fung *et al.* (1992).

In the inertial range and under the assumption of locality (see Fung & Vassilicos 1998), the mean separation of particle pairs scales like

$$\langle \Delta^2(t)\rangle - \Delta_0^2 = G_\Delta \epsilon t^3, \tag{3.5}$$

where Δ_0 is the particle separation at time t_0, $\langle \Delta^2(t)\rangle = \langle |\boldsymbol{\Delta}^2(t)|\rangle$ is the mean-square particle separation at time t, ϵ is the turbulent dissipation rate and G_Δ is a dimensionless universal constant. In figure 4 we summarize the simulation results that we now discuss (see also table 1 for the simulation parameters). A well-defined t^3 scaling over almost 2 decades is observed and we estimate G_Δ to be

$$G_\Delta \approx 0.07.$$

	Setup I	Setup II	Setup III
ω_n	0	0	0
N_k (geometric)	120	120	120
No. of particles	1024	1024	1024
u_{rms}	1	1	1
ϵ	0.54	0.54	0.54
k_η/k_1	10^5	10^3	10^1
η	6.28×10^{-5}	6.28×10^{-3}	6.28×10^{-1}
$\tau_\eta = \epsilon^{-1/3} k_\eta^{-2/3}$	5.70×10^{-4}	1.23×10^{-2}	2.65×10^{-1}

TABLE 1. Simulation parameters for all kinematic simulations (except for the convergence test in figure 3 where N_k has been varied). The 'energy' of the kinematic simulation is normalized such that $(\frac{3}{2})u_{rms} = \int E(k)\,\mathrm{d}k = 1.5$. The parameter ϵ with dimensions of a dissipation rate is then obtained from $\epsilon = u_{rms} C_K^{-3/2} k_1^{-1}$. When using KS alone, u_{rms} and therefore ϵ is an input parameter; when KS is used as a subgrid model (see §4) u_{rms} is derived from the LES field and we denote it $u_{rms,KS}$.

This value for G_Δ agrees well with previous kinematic simulations; Fung *et al.* (1992) estimated an asymptotic value of $O(0.1)$ by investigating different (but all short) sizes of the inertial range; Elliott & Majda (1996) found in their Monte Carlo simulations of fractal flow fields a $G_\Delta = 0.062 \pm 0.008$ with a very large inertial range.

In figure 4(*a*) we present the effect of varying the ratio of the inner to the outer wavenumbers k_η/k_1. The improvement of the t^3 scaling with increasing range of inertial scales in the velocity field is evident. In figure 4(*b*) we investigate the effect of varying the initial separation Δ_0 for the case where $k_\eta/k_1 = 10^5$. The inertial-range behaviour is reached for all cases and it is seen to be broadly speaking independent of the initial separation. For early times, $t/\tau_\eta < 10^2$, where τ_η is defined as $\tau_\eta \equiv \epsilon^{-1/3} k_\eta^{-2/3}$, the most extreme cases $\Delta_0 = 10^{-2}\eta, 10\eta$ display a slightly non-smooth behaviour. This is due to the adaptive time-stepping procedure which can produce rather large variations of the time-step size for times prior to when Richardson's inertial-range scaling is observed. This has however no effect on two-particle statistics in the inertial range as we find by comparison with non-adaptive time stepping for a few selected cases. In figure 5 we find that for both the mean-square separation and the separation p.d.f. (see also §4.4) the differences are within the statistical scatter. One of the simulations, with $\Delta_0 = \eta$, has been left running on the computer for a long time to show that the behaviour for very large times when particle pairs move independently of each other (Thomson 1990), $\langle \Delta^2(t) \rangle \sim t$, is also recovered in KS. We remark that the adaptive time stepping (3.4) destroys this correct long-time scaling and we therefore activate the adaptive time stepping only for $t < T_L$ and apply a constant time step for $t > T_L$ where T_L is the Lagrangian integral time scale of the flow. Indeed for $t \gg T_L$ we have $\langle \Delta^2(t) \rangle \sim t$.

3.3. *Discussion*

We have determined and tested various issues involved in the running of KS (unsteadiness, time-stepping procedure, wavenumber distribution, number of modes), and have confirmed that particle pairs in a three-dimensional homogeneous and isotropic KS velocity field with a $k^{-5/3}$ energy spectrum separate according to Richardson's t^3 law, and that the Richardson constant $G_\Delta \approx 0.07$. Stochastic models of turbulent two-particle dispersion lead to values of G_Δ that depend on the value of the constant C_0, and for the admittedly highly uncertain experimentally obtained value of C_0,

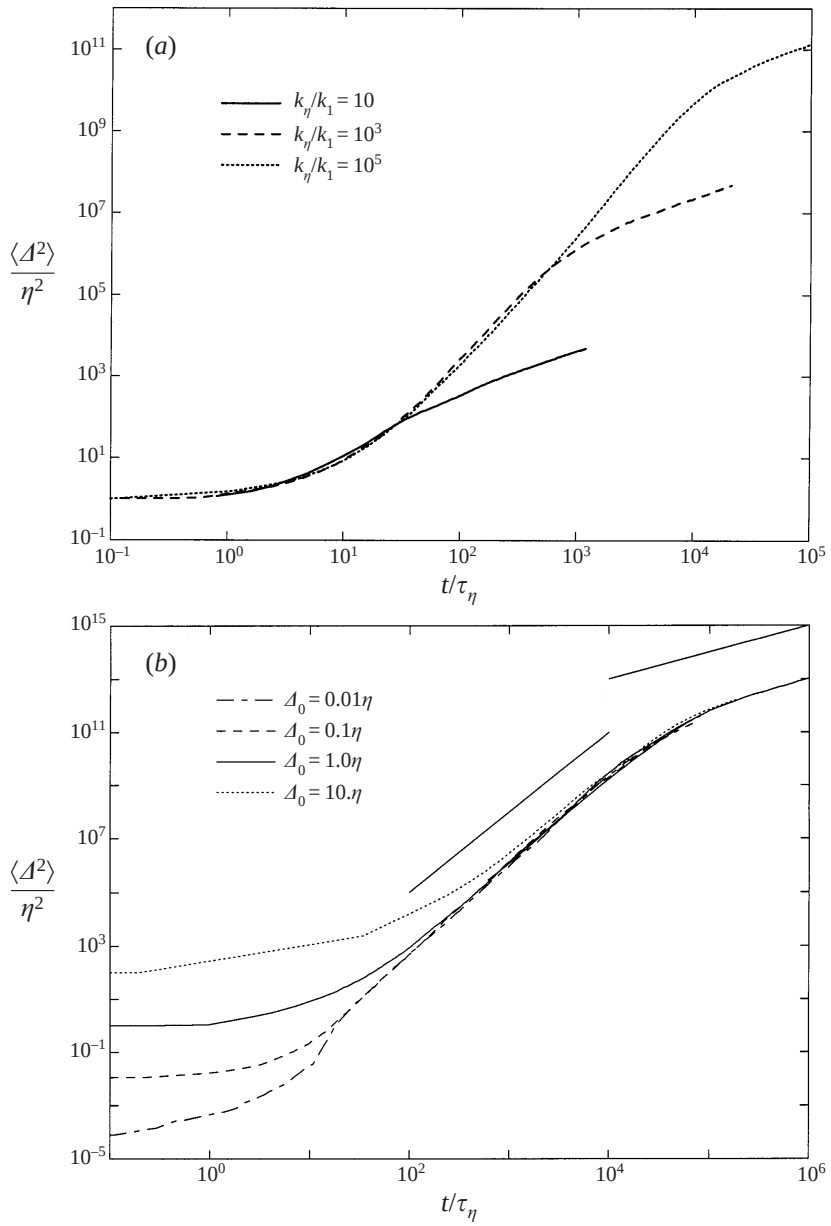

FIGURE 4. Mean-square separation in KS: (*a*) varying size of inertial range $k_\eta/k_1 = 10, 10^3, 10^5$ (initial separation $\Delta_0/\eta = 1$); (*b*) varying initial separation $\Delta_0/\eta = 0.01, 0.1, 1, 10$ (inertial range $k_\eta/k_1 = 10^5$).

$C_0 = 4$, they lead to values of G_Δ that are significantly larger than that of KS (often by one or two orders of magnitude – see Pedrizzetti & Novikov 1994; Heppe 1998; and discussions in Fung & Vassilicos 1998; Fung *et al.* 1992 and Elliott & Majda 1996).

An important drawback of a kinematic simulation is that by construction its Lagrangian integral time scale is imposed. By prescribing a particular energy spectrum for all turbulent scales the Lagrangian integral time scale directly depends on the

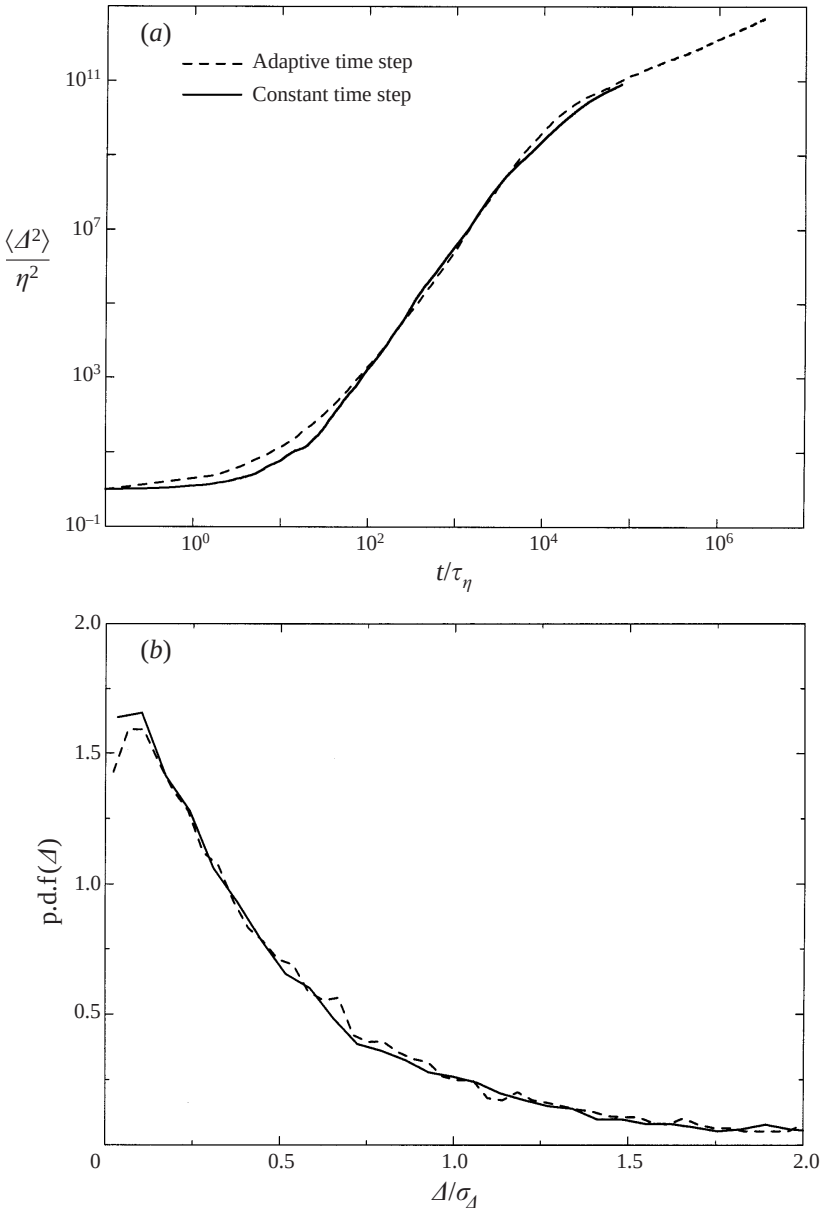

FIGURE 5. The effect of the adaptive time stepping in KS: (*a*) mean-square separation (initial separation $\Delta_0/\eta = 1$) and (*b*) the separation p.d.f. (2.18) in the inertial range at $t/(u_{rms}^2/\epsilon) = 0.1$, see also figure 14 for comparison.

largest (kinematic) turbulent scales. Because the large scales of the turbulence are not included in the KS, this integral time scale is not very accurately predicted. Hence, there is an additional advantage in using KS in conjunction with a large-eddy simulation because the Lagrangian integral time scale can be prescribed by the large-eddy field whilst the kinematic field accounts only for the turbulent small scales.

4. A KS scalar subgrid model

In this section we show how KS can be used as a scalar subgrid model for LES and enable the computation of scalar variances in LES. In § 4.1 we briefly discuss the Lagrangian subgrid models for scalar fields and describe the limitations of previous LES with particles. In § 4.2 details of the new simulation technique are given and in the subsequent subsections we discuss the results obtained by the LES with the KS subgrid model. In § 4.3 we present two-particle dispersion results. In § 4.4 we discuss the relation between two-particle statistics and the scalar variance field and we give one example where we can compute the variance field from particle statistics and we compare the results with experiments.

4.1. *Lagrangian subgrid models for scalar fields*

Instead of considering a continuous scalar field θ we may imagine the passive scalar as consisting of a cloud of particles (or fluid elements), each particle retaining its identity while it follows the flow. For a large number of (sufficiently small) particles, the equivalent of the scalar advection–diffusion equation (1.4) is given by

$$\mathrm{d}\boldsymbol{x} = \boldsymbol{u}\,\mathrm{d}t + \sqrt{2\kappa}\,\mathrm{d}\boldsymbol{W}(t), \tag{4.1}$$

where $\mathrm{d}\boldsymbol{W}(t)$ is a Gaussian white-noise process with zero mean and variance $\mathrm{d}t$, and $\boldsymbol{u}(\boldsymbol{x}(t),t)$ is the Lagrangian velocity at point $\boldsymbol{x}(t)$ and time t. This Lagrangian description of scalar fields has been mostly used in stochastic models of turbulence, and in fact goes back to Taylor (1921) who approximated the effect of turbulent motions by Gaussian white-noise increments to derive a model for the mean concentration field in turbulent flow. For recent accounts of stochastic models see Thomson (1990) or Pedrizzetti & Novikov (1994).

In a LES (4.1) can be written as

$$\mathrm{d}\boldsymbol{x} = (\overline{\boldsymbol{u}} + \boldsymbol{u}')\,\mathrm{d}t + \sqrt{2\kappa}\,\mathrm{d}\boldsymbol{W}(t), \tag{4.2}$$

where $\boldsymbol{u}'$ is the (unknown) subgrid velocity field that needs to be modelled to obtain a solution for the passive scalar field.

Equation (4.2) has been applied to LES in dispersion studies in the atmospheric boundary layer (e.g. Mason 1992; Hadfield 1994; Kemp & Thomson 1996). However, in all these studies the subgrid velocity field was modelled by a white noise with a given eddy diffusivity κ_t, i.e. $\boldsymbol{u}'\,\mathrm{d}t = \sqrt{2\kappa_t}\,\mathrm{d}\boldsymbol{W}(t)$ and therefore

$$\mathrm{d}\boldsymbol{x} = \overline{\boldsymbol{u}}\,\mathrm{d}t + \sqrt{2\kappa_t}\,\mathrm{d}\boldsymbol{W}(t), \tag{4.3}$$

where molecular diffusion effects have been neglected because $\kappa_t \gg \kappa$. The choice of κ_t in these studies was, as usual, based on the assumption of a constant turbulent Prandtl number.

Equation (4.3) is in fact the equivalent of the filtered scalar advection–diffusion equation (1.6) where the gradient-diffusion assumption (1.8) has been used and κ is neglected in front of κ_t. However, in the present LES, we use (4.2) instead of (4.3) and therefore make no gradient-diffusion assumption for the scalar field. Instead, we assume the KS form (3.1) for the subgrid velocity $\boldsymbol{u}'$ which means that $\boldsymbol{u}'$ is incompressible, compatible with Kolmogorov scaling and contains subgrid flow structure. It also means that, although $\boldsymbol{u}'$ is not accurate in the Eulerian frame, it does generate accurate Lagrangian statistics as demonstrated by Malik & Vassilicos (1999) and our results in § 3. The alternative gradient-diffusion strategy whereby the subgrid velocity field is modelled by a white noise enhances one-particle diffusion but the

N	Box size	k_c/k_0	u_{rms}	L	T_L	T_E	$\bar{\epsilon}$	σ_ϵ
32	2π	15	1	1.13	1.2	1.14	0.43	0.037

TABLE 2. The simulation parameters of the velocity LES. The low-energy modes $|\boldsymbol{k}| \leqslant 2.5$ are forced such that the total energy $E = \int_{k_1}^{k_c} E(k)\,\mathrm{d}k$ is kept constant with $E = 1.5$. The mean dissipation rate is obtained from $\bar{\epsilon} = -\langle \mathrm{d}E/\mathrm{d}t \rangle$, and its variance is defined by $\sigma_\epsilon^2 = \langle (\bar{\epsilon} - \epsilon(t))^2 \rangle$. L is the turbulent integral length scale, T_L is the Lagrangian integral time scale and T_E is the eddy turnover time. $k_0 = 2\pi/(\text{box size}) = 1$ in arbitrary units denotes the smallest wavenumber of the simulation.

scaling effects of the inertial subgrid range on two-particle statistics are lost. When the subgrid velocity $\boldsymbol{u}'$ is modelled by KS such effects are included and two-particle statistics display inertial scaling as well (see § 3).

The mean scalar field is mainly determined by the large turbulent scales which contain most of the turbulent kinetic energy, and it is therefore to be expected that a simple model like (4.3) which adds only some additional randomness to the large-scale turbulence is sufficient to predict the mean concentration field. On the other hand, the mean concentration variance is largely determined by the (self-similar) structure of the turbulent small scales and a Gaussian white noise is clearly not appropriate to represent a Lagrangian velocity field that can generate two-particle inertial-range Richardson scaling. Indeed, whereas the studies of Mason (1992) and Hadfield (1994) showed results for the mean spreading behind point sources, no estimates for the variance field could be given. In this study we propose an approach which does not rely on an eddy diffusivity like (4.3) but models (4.2) with KS. Accordingly, our model allows us to compute $\langle \theta^2(\boldsymbol{x}, t) \rangle$, i.e. the mean variance field (given the assumptions of the model), whereas the eddy diffusivity allows only the (insufficient) approximation $\langle \bar{\theta}^2(\boldsymbol{x}, t) \rangle$ to be computed.

4.2. *KS as a scalar subgrid model for LES*

We propose to use the kinematic random velocity field from § 3 as an approximation of the filtered subgrid field,

$$\mathrm{d}\boldsymbol{x} = (\bar{\boldsymbol{u}} + \boldsymbol{u}_{KS})\,\mathrm{d}t \tag{4.4}$$

with $\boldsymbol{u}_{KS}$ being the approximation for $\boldsymbol{u}'$ in (4.2), and where molecular diffusion effects have been neglected.

We use in this study a spectral LES of stationary isotropic turbulence for the velocity field $\bar{\boldsymbol{u}}$, see table 2. To obtain stationarity a low-mode forcing is employed for $0.5 \leqslant k/k_0 < 2.5$, such that the rate of energy input by the forcing is equal to the energy lost in the previous time step so that the overall energy in the field is kept constant. k_0 is the smallest wavenumber of the LES which in our case for a domain size of 2π in arbitrary units is $k_0 = 1$; this wavenumber should not be confused with any of the wavenumbers $k_n = k_1 \ldots k_{N_k}$ of the KS field.

In figure 6 we show schematically in wavenumber space how this model adds the filtered subgrid scales to the resolved scales. Provided the LES is defined by a sharp Fourier cutoff wavenumber k_c that is within the inertial range of scales, we can add the subgrid velocity field with the appropriate amplitude at the cutoff. The lowest wavenumber k_1 of the KS subgrid field is set equal to the cutoff wavenumber k_c of the LES, $k_1 = k_c$. Whereas the modes $k < k_c$ are correlated via the evolution of the velocity field in the large-eddy simulation, none of the modes $k > k_c$ are correlated with each other but chosen independently from each other in the kinematic field.

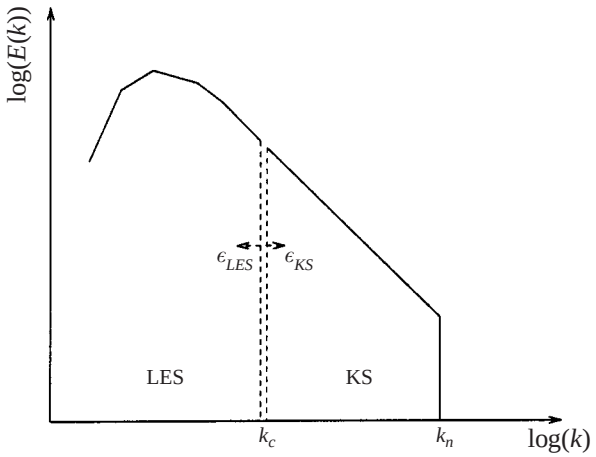

FIGURE 6. Sketch of the coupling between LES and kinematic subgrid model. The LES is assumed to have a sharp Fourier cutoff at k_c, with k_c being within the inertial range of scales. The coupling is made by matching the parameter ϵ_{KS} of the KS field with dimension of a dissipation rate to the dissipation rate in the LES field $\epsilon_{LES} = -\mathrm{d}E(t)/\mathrm{d}t$, $\epsilon_{LES} = \epsilon_{KS}$.

Therefore, we do not try to correlate any of the kinematic modes with the large-eddy field.

The coupling between the turbulent large and small scales is made purely at the energy level by matching the rates of dissipation. We estimate the dissipation rate in the LES field by

$$\epsilon_{LES} = -\frac{\mathrm{d}E(t)}{\mathrm{d}t}. \tag{4.5}$$

where $E(t)$ is the total kinetic energy of the large-scale (supergrid) velocity field at time t, and we set this value of ϵ_{LES} equal to the parameter ϵ_{KS} in the subgrid energy spectrum (3.2) at every time step. We have added the subscripts here to clarify to the reader what the two different ϵ that we define in this study are. Another possibility to obtain a value for the dissipation rate of the LES would be to assume Kolmogorov scaling at the cutoff wavenumber k_c, and thus for the dissipation rate to be $\epsilon_{LES} = (E(k_c)k_c^{5/3}/C_K)^{3/2}$. However this is likely to be more influenced by the accuracy of the velocity subgrid model at the cutoff. As discussed by Lesieur & Métais (1996), the spectral eddy viscosity (1.11) may not be expected to be very accurate near the cutoff wavenumber and we therefore prefer to estimate the dissipation rate by using (4.5).

From (3.2) we find that

$$\begin{aligned}\epsilon_{KS} &= \left[\frac{2}{3}\int_{k_c}^{k_\eta} E(k)\,\mathrm{d}k\, C_K^{-1}\left(k_c^{-2/3} - k_\eta^{-2/3}\right)^{-1}\right]^{3/2} \\ &\approx \left[u_{rms,KS}^2\, C_K^{-1}\, k_c^{2/3}\right]^{3/2},\end{aligned} \tag{4.6}$$

where $(\frac{3}{2})\,u_{rms,KS}^2 = \int_{k_c}^{k_\eta} E(k)\,\mathrm{d}k$ is the energy contained in the KS subgrid field. Numerically, we set $\epsilon_{KS} = \epsilon_{LES}$ at every time step and adjust the subgrid-scale energy $(\frac{3}{2})\,u_{rms,KS}^2$ by rescaling the amplitudes $\boldsymbol{a}_n$ and $\boldsymbol{b}_n$ in (3.1). The simulation procedure is as follows. The random structure of the subgrid velocity field is selected at $t = 0$ once and for all. Then, as the simulation proceeds, i.e. as the tracer particles are advected

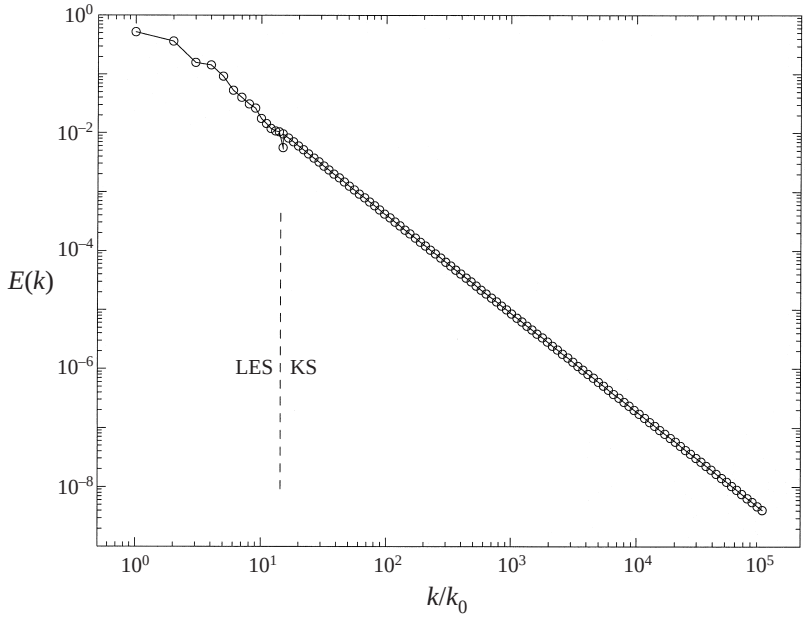

FIGURE 7. Energy spectrum of LES with KS subgrid model. The LES consists only of a very short range of wavenumbers, $1 \leqslant k/k_0 \leqslant k_c/k_0 = 15$. The KS model adds a well-defined inertial range of scales with $15 \leqslant k/k_0 \leqslant 10^5$.

through the turbulence, the amplitudes a_n, b_n are rescaled at each time step according to the mean dissipation rate $\epsilon(t)$ that is obtained from the velocity LES. In table 2 we give the numerical values of both the mean dissipation rate $\overline{\epsilon}$ and its variance $\sigma_\epsilon^2 = \langle(\overline{\epsilon} - \epsilon(t))^2\rangle$, where the brackets denote time averages.

Figure 7 depicts a typical energy spectrum of the complete flow field $\boldsymbol{u} = \overline{\boldsymbol{u}} + \boldsymbol{u}_{KS}$ with $k_c/k_0 = 15$. For $k/k_0 \leqslant 15$ (with $N = 32^3$ grid points) the velocity field is given by the LES simulation with the spectral eddy viscosity (1.11), and in the range $15 \leqslant k/k_0 \leqslant 10^5$ we add the kinematic flow field with Kolmogorov's $k^{-5/3}$ inertial-range scaling. The coupling between ϵ_{LES} and ϵ_{KS} is adjusted at every time step, the fluctuations are very small however. It is seen that the KS field smoothly extends the short inertial scaling of the LES field towards a large range of scales.

The definition of a LES based on the spectral eddy viscosity is formally valid in the limit $Re \to \infty$. Using KS as a scalar subgrid model introduces explicitly a minimal turbulent scale $\eta = 2\pi/k_\eta$ and a finite Reynolds number may be defined as $Re \sim (L/\eta)^{4/3}$ in accordance with Kolmogorov's inertial-range equilibrium theory. We stress that in this way we include finite Reynolds number effects in the scalar statistics, but not in the velocity field dynamics.

A serious simplification made in the present model is the abrupt decimation of the wavenumber density across the cutoff k_c. Whereas the LES has many modes in its outer shell at k_c, the KS subgrid field has only a single mode in every shell and the shell spacing is increased as well. This abrupt change was not evident in any of the particle statistics that we traced. The two-particle dispersion statistics appear very insensitive to the change in wavenumber density across k_c. Malik & Vassilicos (1999) have shown recently that KS alone is able to reproduce the Lagrangian two-particle statistics obtained from DNS (Yeung 1994). They used energy spectra similar to those of the DNS study but with a dramatic reduction in the number of Fourier modes

	Setup I	Setup II	Setup III	Setup IV
Subgrid model	KS	KS	White noise	No model
No. of particles	1024	1024	1024	1024
k_η/k_0	10^5	10^3	—	—
k_c/k_0	15	15	—	—
η	6.28×10^{-5}	6.28×10^{-3}	—	—
$\tau_\eta = \epsilon^{-1/3} k_\eta^{-2/3}$	6.13×10^{-4}	1.32×10^{-2}	—	—
Pr_t	—	—	0.6	—

TABLE 3. The scalar subgrid model setup. The LES from table 2 is used as a supergrid field ($k/k_c \leqslant 15$), and the KS or white noise velocities are added for the subgrid scales ($k/k_c > 15$), see also (4.4) and (4.3). $k_1 = k_c$ is the smallest wavenumber in the KS subgrid model. The white noise subgrid model is based on a turbulent Prandtl number Pr_t where we use $Pr_t = 0.6$ in agreement with § 1.2.

by a factor of four orders of magnitude! We conclude that the results of Malik & Vassilicos (1999) are consistent with what we find here.

The numerical implementation of the KS scalar subgrid model is done by embedding the particle advection scheme in the time stepping of the large-scale (supergrid) flow field. This is due to the added turbulent small scales which put an additional restriction on the time step size. The time step size for the velocity field $\mathrm{d}t_u$ is given by the numerical stability condition of the LES. The time step size for the particle pairs is given by the adaptive time step $\mathrm{d}t_a$ in (3.4). The actual step size for the particles $\mathrm{d}t_p$ is the smallest of these two step sizes, i.e. $\mathrm{d}t_p = \min[\mathrm{d}t_a, \mathrm{d}t_u]$. If $\mathrm{d}t_a < \mathrm{d}t_u$, an embedded inner time stepping loop exists during which the supergrid field is kept constant ('frozen'). This is a reasonable approximation because the turbulent large scales contained in the LES field vary over much larger time scales. In fact, it is important to note that the adaptive time step is only active over a short initial range of times. For times $t/\tau_\eta > O(1)$ (see figure 8*b*) we find that $\mathrm{d}t_a > \mathrm{d}t_u$ and the step size is limited by the numerical stability of the LES only. The velocity field is advanced with a second-order Runge–Kutta method. If $\mathrm{d}t_a < \mathrm{d}t_u$, the additionally embedded time-integration method for the particles is a simple Euler forward. The choice of this most simple method for the particle advection is motivated by numerical cost only. However, tests were performed in KS alone with different integration methods and no improvements on particle statistics could be identified with higher-order methods.

4.3. *Two-particle dispersion*

Having demonstrated that KS is capable of producing, in terms of two-particle statistics, a reasonable inertial-range flow field, we turn to the coupling of kinematic fields with LES. The relevant simulation parameters are summarized in tables 2 and 3. To obtain the Lagrangian supergrid velocities an interpolation procedure is necessary and different methods have been tried. No significant difference between simple linear interpolation and the more accurate cubic spline interpolation could be identified, and we present here results based on linear interpolations to obtain the LES supergrid Lagrangian velocities.

The performance of the model in terms of two-particle statistics is depicted in figures 8 and 9. Figure 8 shows, similarly to figure 4(*a*), the effect of different sizes of the inertial subrange. Figure 8(*a*) displays the two-particle statistics normalized with turbulent integral scales L and T_L and the converging long-time behaviour due to

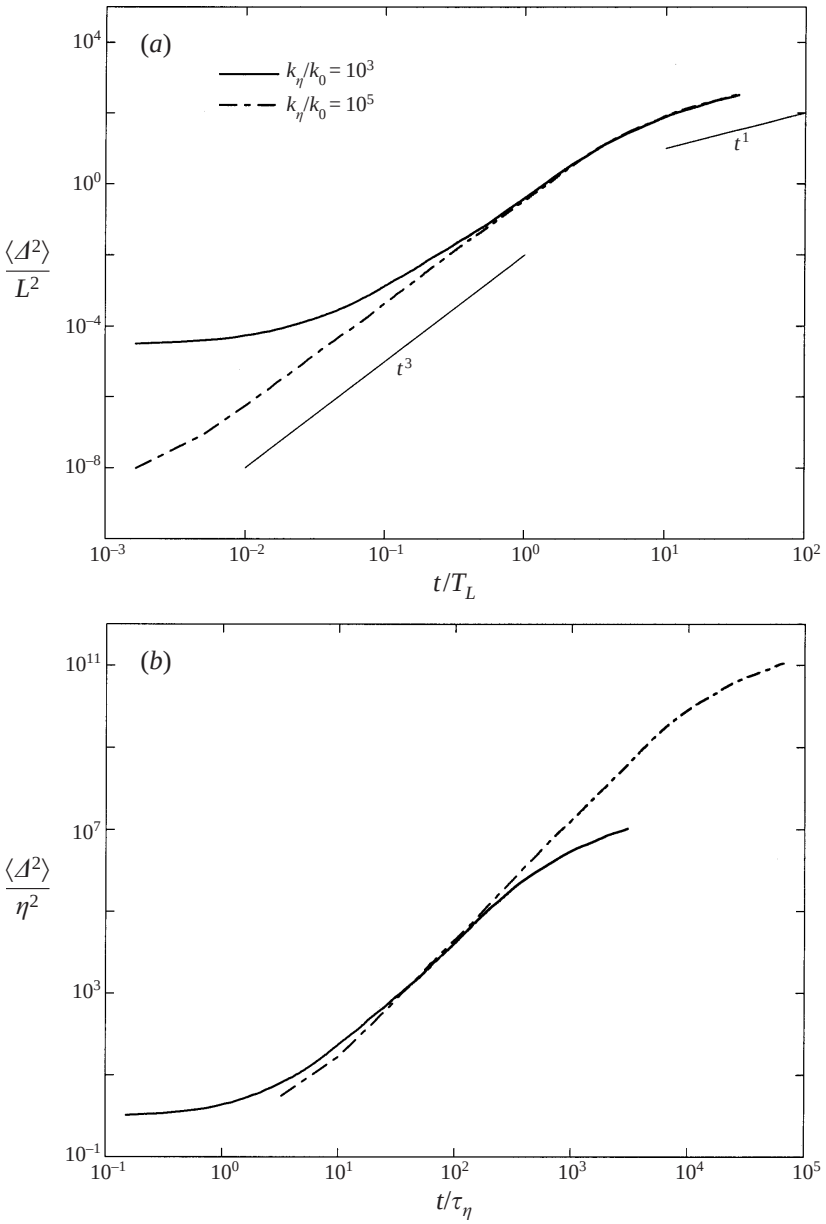

FIGURE 8. Mean-square separation in LES for two different sizes of the KS inertial range, $k_\eta/k_0 = 10^3$, 10^5; initial separation $\Delta_0/\eta = 1$: (*a*) normalized with outer variables; (*b*) normalized with inner variables.

the LES field (independent of the size of the inertial range) is visible. Figure 8(*b*) uses the Kolmogorov scales η and τ_η for normalization as has been used in figure 4.

Figure 9 is added to show the effect on two-particle statistics of the subgrid velocity field $\boldsymbol{u}'$. The solid line shows the correct scaling behaviour using the kinematic subgrid field. When using no subgrid field at all, we lose all the small eddying and straining structures that tear the particles apart and as a consequence the initial separation remains unaltered over a large range of times. It is only at very late times that the

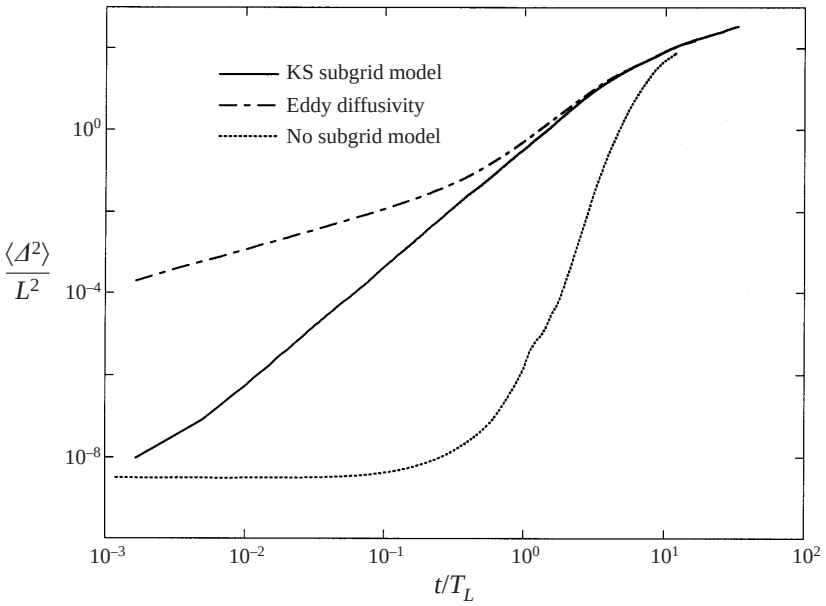

FIGURE 9. The effect of the KS subgrid model on the mean-square separation in LES is shown by comparison to a simple eddy diffusivity model (where particle pairs move independently in the inertial range) and no subgrid model (where particle pairs are on average moving only apart when they are on integral scales).

effect of the large-scale turbulent motion is felt and the separation quickly increases to approach the correct long-time behaviour dominated by the large scales. In the case of an eddy diffusivity model (4.3) with $Pr_t = 0.6$ it is seen that the added Brownian motion acts also at small scales and results in t^1 scaling, followed by a short range during which the inertial effects of the LES scales are weakly felt before the particles again move independently apart for $t \gg T_L$.

The results shown here are very similar to those of § 3.2. The important difference is in the integral scales of the flow. Whereas the integral scales in a purely kinematic flow field are determined by the model itself, it is now the LES which determines the integral scales. In fact, if we estimate the Lagrangian integral time scale from KS alone ($T_L = 0.65$, see figure 3), one obtains a value that is significantly lower than the one obtained from the coupled simulation ($T_L = 1.2$, see table 2). Importantly, both experiments and DNS support the higher value, i.e. $T_L u_{rms}/L \approx 1$ (see Fung *et al.* 1992; Snyder & Lumley 1971; Durbin & Hunt 1980 and Yeung & Pope 1989).

4.4. *Separation p.d.f. and the scalar variance*

We now use the KS subgrid model to compute scalar variance statistics. A numerical estimate of the variance field has to rely on a number of assumptions as explained in § 2 and we first validate these assumptions before presenting results on the two-particle p.d.f. In a first step we show that the forward integration is possible for two-particle statistics in KS. We then validate for our LES+KS model Sawford's assumptions introduced in § 2.2. Finally, using the LES+KS model we calculate the two-particle p.d.f.s and the scalar variance field of an instantaneous line source.

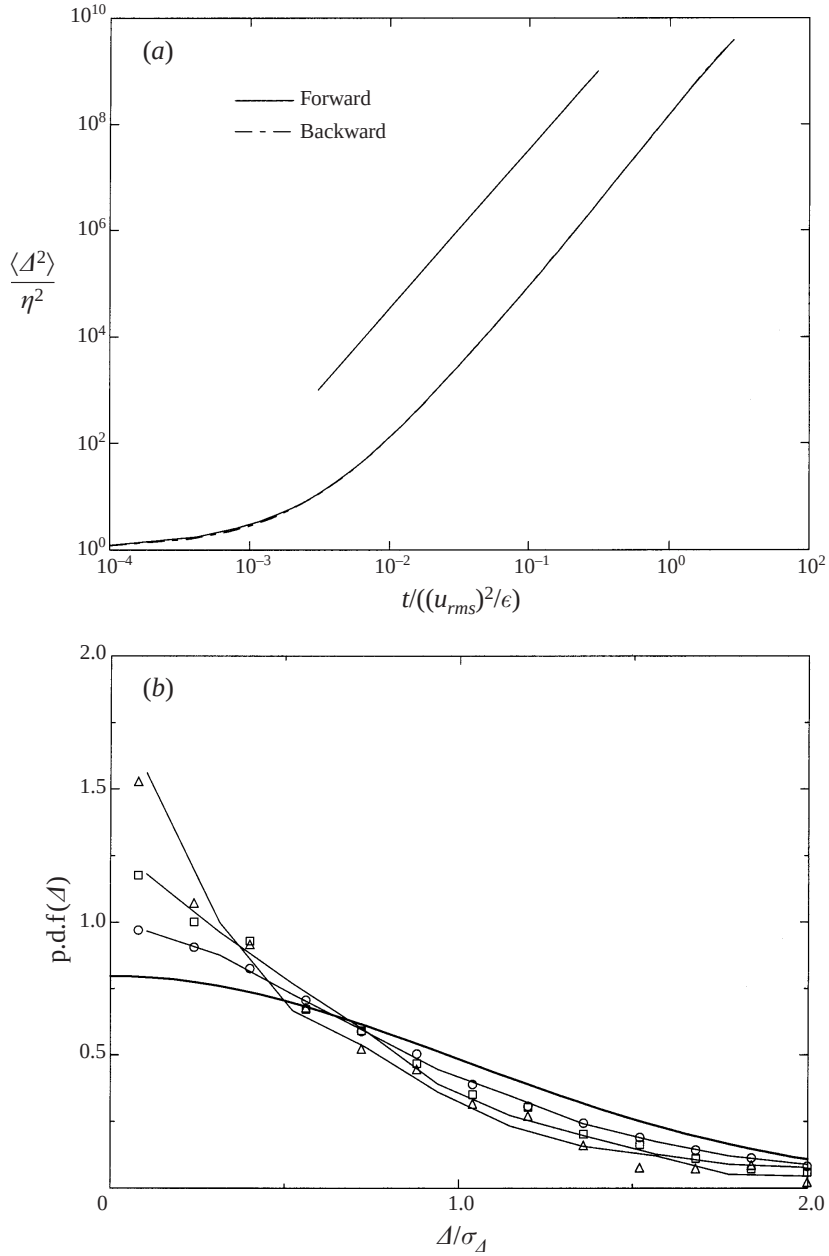

FIGURE 10. By integrating backwards and forwards in time we investigate the reversibility of the KS model. (*a*) For the mean-square separation virtually no difference between forwards and backwards integration is evident. (*b*) The separation p.d.f.s (2.18), (2.19) at one example of an instant of time during the inertial range of times, and normalized with the mean-square separation. The lines are obtained from a forward simulation, i.e. $t/(u_{rms}^2/\epsilon) = 0.1$, and the symbols correspond to a backward simulation with $t/(u_{rms}^2/\epsilon) = -0.1$. The difference between forward and backward integration is within the statistical scatter.

Forward diffusion

It was mentioned that the separation p.d.f.s for forward and backward diffusion cannot *a priori* be expected to be the same. The calculation of the scalar variance is based on the very impractical $p_\Delta(\boldsymbol{\Delta}_0, t; \boldsymbol{\Delta}', t_0)$, see (2.14). As was explained in § 2.2, in stochastic models one therefore simply integrates backwards in time (see (2.16)) which for example in the case of a decaying turbulence field would lead to an increasing turbulence intensity as time advances. Even for a statistically stationary turbulence, integrating LES of the Navier–Stokes equations backwards in time is not possible. We can reasonably assume however that for particle separations below the integral scale the particle statistics are dominated by the kinematic subgrid model. Because the kinematic model is based on a summation of Fourier modes we are able to integrate forwards and backwards in time when using the kinematic field alone. In this way, we can investigate the effect that time-reversal has on our model. In figure 10 we show results for the mean-square separation and for the separation p.d.f.s p_Δ, $\overline{p}_\Delta$ and $\overline{\overline{p}}_\Delta$ ((2.18) and (2.19)), integrating forwards and backwards in time for a kinematic field where the turbulent kinetic energy $(\frac{3}{2})u_{rms}^2$ is kept constant in time. The mean-square separation is almost identical, and only for very short times $t/(u_{rms}^2/\epsilon) < 10^{-2}$ are the two curves barely distinguishable. The three p.d.f.s are selected at one instant of time within the inertial time range $t/(u_{rms}^2/\epsilon) = 10^{-1}$. The lines are obtained from a forward integration and the symbols correspond to the backwards simulation. No difference can be seen within the statistical scatter. We therefore conclude that for our model we may assume $p_\Delta(\boldsymbol{\Delta}', t_0; \boldsymbol{\Delta}_0, t) = p_\Delta(\boldsymbol{\Delta}', t; \boldsymbol{\Delta}_0, t_0)$. This enables us to validate Sawford's assumptions for this LES+KS model and to compute various p.d.f.s and scalar variances from a forward simulation.

Validating Sawford's assumptions

Sawford's assumptions greatly simplify the computations of the mean concentration and concentration variance fields, see (2.13) and (2.14). The first assumption is that $\boldsymbol{\Delta}$ and $\boldsymbol{z}$ are independent and in figure 11 we report a computation of three components of the correlation tensor $\mathrm{Corr}(\Delta_i, z_j) = (\langle \Delta_i z_j \rangle - \langle \Delta_i \rangle \langle z_j \rangle)/(\langle \Delta_i^2 \rangle \langle z_j^2 \rangle)^{1/2}$. No significant correlation between $\boldsymbol{\Delta}$ and $\boldsymbol{z}$ has been observed. A more stringent test of the assumption of statistical independence between $\boldsymbol{\Delta}$ and $\boldsymbol{z}$ is shown in figure 12 where we plot the separation p.d.f. p_Δ conditional on different absolute values of the centre of mass z. The unconditional p.d.f. p_Δ is discussed below in more detail where it is also plotted for different times (see figure 14*a*). We pick here a time within the inertial range, $t/(u_{rms}^2/\epsilon) = 0.1$, to test the statistical independence of $\boldsymbol{\Delta}$ and $\boldsymbol{z}$ in this range. It should be pointed out that the conditional separation p.d.f. is numerically expensive to compute because it requires the computation of p_Δ for various values of $|\boldsymbol{z}|$. Indeed, figure 12 is obtained from 100 realizations of the flow, each of them with 1024 particles. We use KS without the large-scale LES in this test to keep the computing time reasonable. However, as Sawford's assumption is primarily made for the inertial range where the KS flow structure dominates the particle statistics, we expect no difference if LES turbulent large scales are added to the flow. The conditional p.d.f. is computed by averaging over bands in z of band-width $z_{max}/10$. Even so, the p.d.f.s are noisy, in particular for high values of z/z_{max} where less samples are taken. But as is evident from the plot, they all show the same trend independently of absolute values of $|\boldsymbol{z}|$ and the shape of the p.d.f.s is in good agreement with Thomson (1990).

The second assumption is the Gaussianity of the single-particle p.d.f. $P_1(\boldsymbol{x})$ and

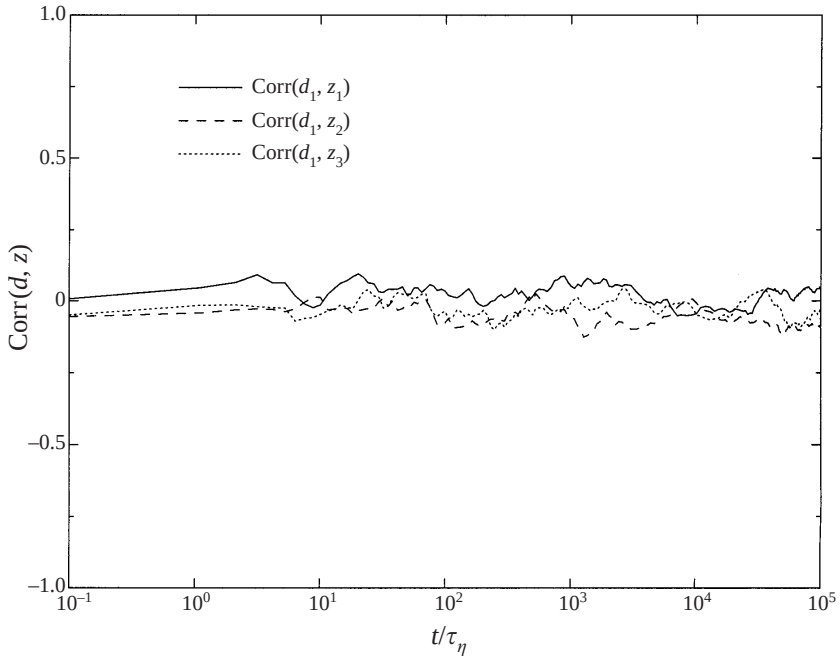

FIGURE 11. The correlation functions $\mathrm{Corr}(\Delta_i, z_j) = (\langle \Delta_i z_j \rangle - \langle \Delta_i \rangle \langle z_j \rangle)/(\langle \Delta_i^2 \rangle \langle z_j^2 \rangle)^{1/2}$ for Δ_1 and z_1, z_2, z_3, taken from a LES+KS simulation with setup I and initial separation $\Delta_0 = \eta$. They are approximately zero for all times and thus support Sawford's assumption of statistical independence of $\boldsymbol{\Delta}$ and $\boldsymbol{z}$.

of the centre-of-mass p.d.f., $p_z(\boldsymbol{z})$. We also tested this assumption in our simulations and in figure 13 it is shown that no significant deviation from Gaussianity can be observed, neither in the inertial range nor for very long times.

The separation p.d.f.

In figure 14(*a*) we show the separation p.d.f. (2.18) as a function of the separation $\Delta' = \Delta'_x$ for different times, in the inertial time range $t/(u^2_{rms}/\epsilon) = 0.1, 1$ and for the large time $t/(u^2_{rms}/\epsilon) = 10$. It is seen that in the inertial time range the p.d.f. is non-Gaussian and roughly constant, and approaching Gaussian behaviour for large times. This is in agreement with Thomson (1990), and we include his numerical results, taken from his figure 1 for comparison. We stress that the good agreement with Thomson's data concerns the (non-Gaussian) shape of the separation p.d.f. only. The absolute values of separation are higher in Thomson's stochastic model due to his higher value of G_Δ; in other words, the non-Gaussianity is more pronounced in the kinematic model if the separation vector is not normalized.

Figures 14(*b*) and 14(*c*) depict the p.d.f.s of the separation vector where averaging was performed over one and two space directions, respectively, (2.19). As seen above, the shape of the particle separation p.d.f.s is of crucial importance when relating particle statistics to the concentration field. We presented here numerical results of these p.d.f.s from simulations where the kinematic flow field has been coupled with LES. However, because the inertial-range behaviour is dominated by the kinematic subgrid field the statistics presented in this section could in principle be obtained by kinematic simulations alone, in which case the Lagrangian integral scale T_L and the dissipation rate ϵ would not be prescribed by the LES but would be 'free'

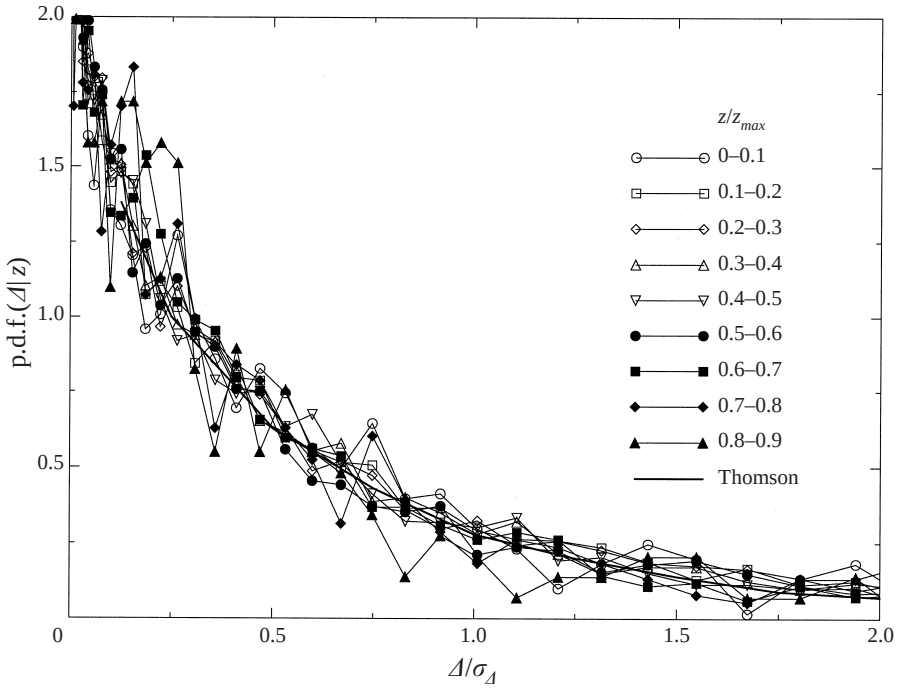

FIGURE 12. The separation p.d.f. p_Δ conditional on different absolute values of the centre of mass z, shown here for a time within the inertial range, $t/(u_{rms}^2/\epsilon) = 0.1$, and normalized by the mean-square separation. The conditional p.d.f. is computed by averaging over bands in z of band-width $z_{max}/10$. This is a stringent test of Sawford's independence assumption and it is found that p_Δ is indeed independent of values of the centre of mass.

input parameters for the model flow. Indeed, the normalized p.d.f.s obtained from kinematic simulations alone (shown in figure 10*b*) have the same shape as for large-eddy simulations with the kinematic model included. However, it is important to note that the coupling of the KS subgrid field with the LES simulation removes the free choice of the integral scale and dissipation rate.

Concentration variances

To compute the scalar mean and scalar variance fields one needs to compute the particle and particle separation p.d.f.s, as well as the variances σ_x, σ_z, see (2.13) and (2.14). We also compute the variance of the particle separation, σ_Δ which is given by $\sigma_\Delta^2 = (\frac{1}{3})\langle\Delta^2(t)\rangle$, to properly rescale the particle separation p.d.f. in (2.14).

The growth of the variances σ_x, σ_z, σ_Δ in time is shown in figure 15. As expected, $\sigma_x \sim t^1$; $\sigma_z = 2\sigma_x$ during the inertial range of times, and $\sigma_x \sim t^{1/2}$; $\sigma_z, \sigma_\Delta \to 2^{1/2}\sigma_x$ for very large times. This behaviour agrees well with the predictions from stochastic modelling, see figure 3 in Thomson (1990) (note that his definition of particle pairs is slightly different from ours). As a practical example of using these particle statistics to determine the concentration variance field we compare in figure 16 our simulations with the experiments of Fackrell & Robins (1982) who measured the concentration variance behind a continuous elevated point source far from the boundary in boundary layer turbulence. In the same figure we included the numerical results of the stochastic model of Thomson (1990). To compute the scalar variance we follow Thomson (1990) who approximated the experimental configuration by an instantaneous line source.

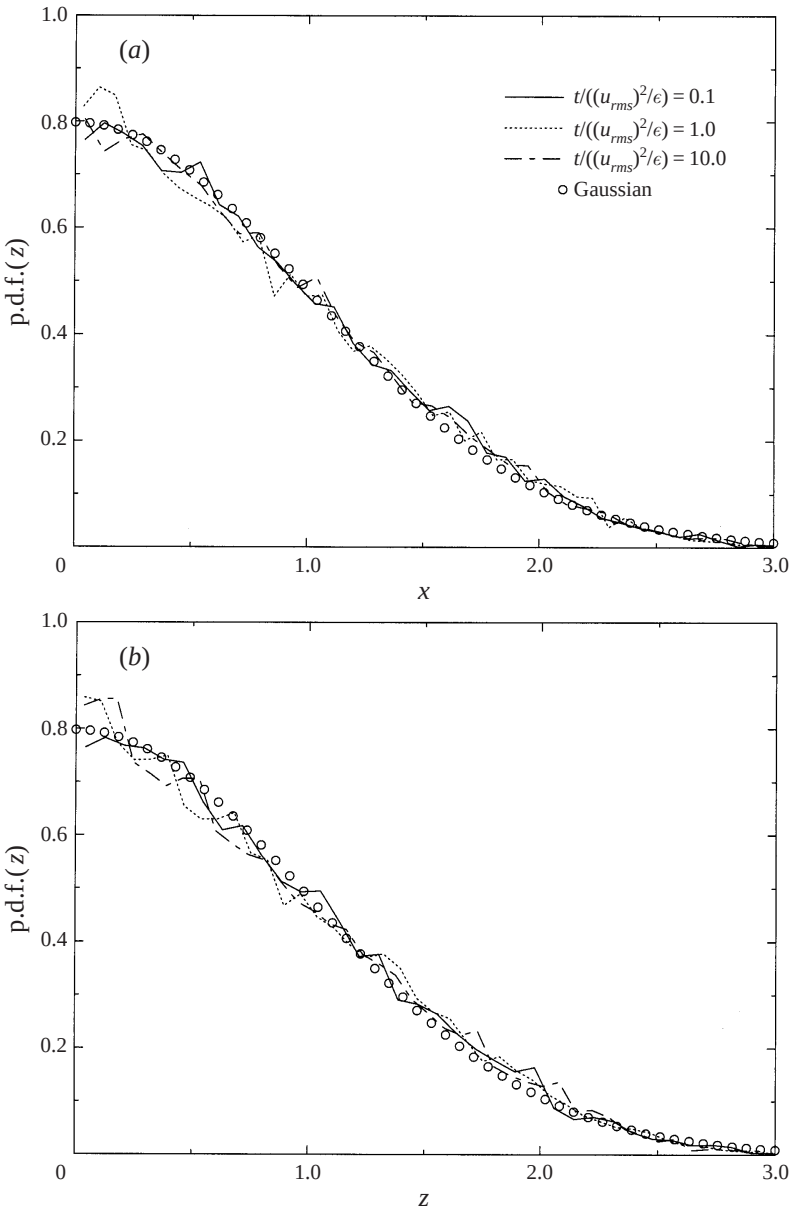

FIGURE 13. Normalized p.d.f.s of (*a*) the particle position and (*b*) the centre of mass of particle pairs for a LES+KS simulation. They are Gaussian for all times which gives support to Sawford's approximations.

The concentration variance is defined by

$$\sigma_\theta = \langle \theta^2 \rangle - \langle \theta \rangle^2. \tag{4.7}$$

Using (2.13) and (2.14) and taking into account the isotropy of $\overline{p_\Delta}$, we can write

$$\sigma_\theta = \left[\frac{\left(2\pi(\sigma_x^2 + \sigma_0^2)\right)^2}{\sigma_z^2 + \sigma_0^2} \int_0^\infty \overline{p_\Delta}(\Delta) G_2(\Delta, \sigma_0) \Delta \, \mathrm{d}\Delta - 1 \right]^{1/2}. \tag{4.8}$$

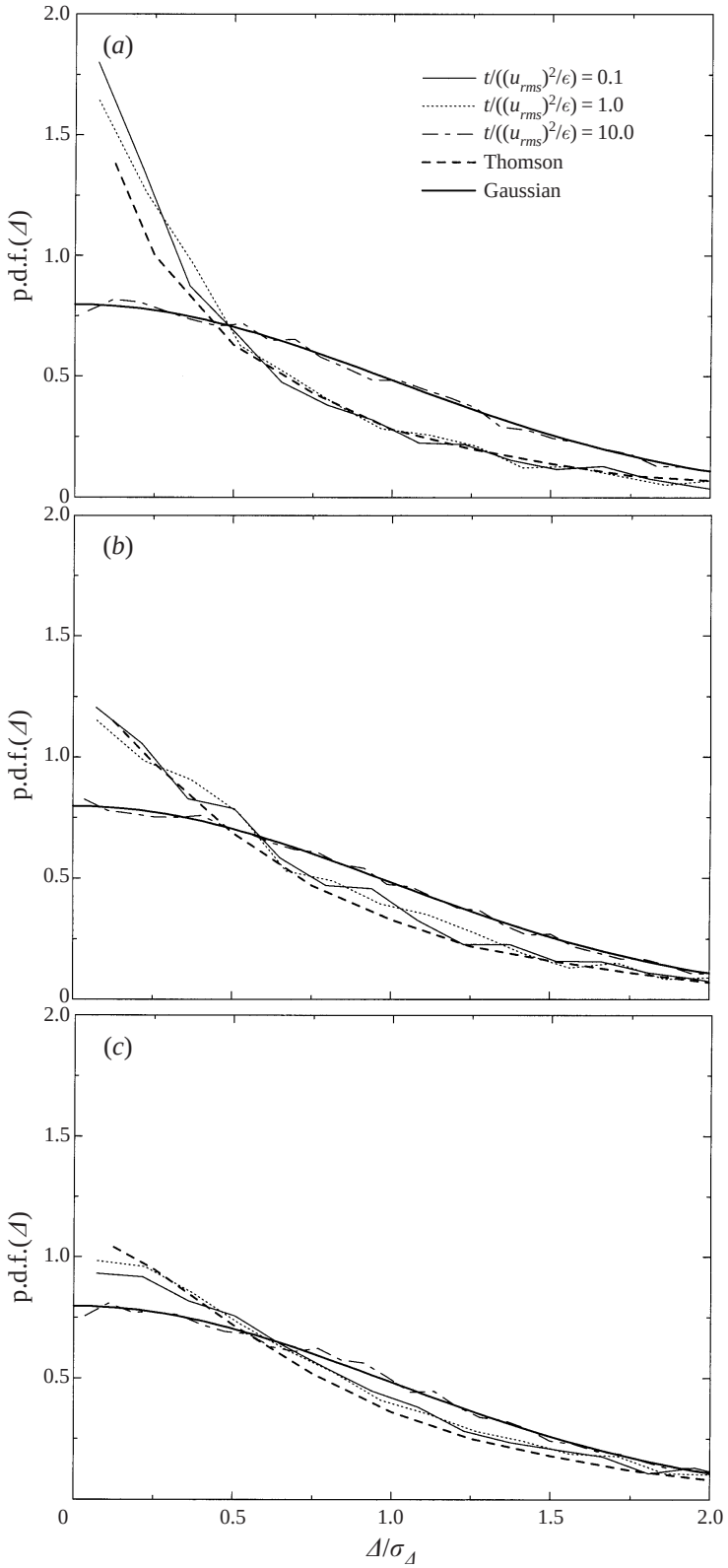

FIGURE 14. For caption see facing page.

Numerically integrating (4.8) for selected times and selected point source sizes we find the results presented in figure 16.

As seen in figure 16, there is some scatter in the experimental data from Fackrell & Robins. There are additional uncertainties which arise from approximating the continuous point source by an instantaneous line source. Moreover, the description of the experimental source with a given nozzle diameter d as a Gaussian with variance σ_0 may be problematic. Indeed, in another study based on a similar stochastic model (Borgas & Sawford 1996) σ_0 was chosen to be slightly smaller than the nozzle diameter. Here we use a σ_0 which equals the nozzle diameter as in Thomson (1990). In view of all these uncertainties, the agreement between experiments and both the kinematic subgrid model and the stochastic model is good and within the scatter of the experimental data.

The difference, however, is that Thomson (1990) needs to pick 'arbitrarily' a value for the Lagrangian constant C_0 which we need not. He chooses $C_0 = 4$ which he motivates by referring to experiments. In fact, Sawford (1991) attributed variations in C_0 to Reynolds number effects in laboratory dispersion. Borgas & Sawford (1996) state that "C_0 is not known with any certainty" and they in fact suggest using higher values for C_0 ($C_0 \approx 6$ or bigger) when they compare their numerical results with another set of experiments. They also demonstrate that a higher value of C_0 leads to an increase of the maximum scalar variance and the quantitative differences are significant. It is therefore advantageous to have a model that does not require an input value for C_0.

Effectively, C_0 contributes in determining the Lagrangian integral time scale which is an input parameter for the stochastic model. In the KS subgrid model the integral time scale is given by construction, in fact by the velocity LES, and the results that we present here are therefore free of any highly uncertain parameters. Indeed, if we estimate C_0 in our simulations by $C_0 = 2u_{rms}^2/(T_L\epsilon)$ (Pope 1994), it is found from the LES that $C_0 = 3.9$, in agreement with the expectation from experiments.

Finally, we remark that another important difference between stochastic models and kinematic flow fields is their incompressibility in an Eulerian frame. A KS field is incompressible by construction whereas enforcing incompressibility for a stochastic model is highly non-trivial (Thomson 1990; Pedrizzetti & Novikov 1994).

5. Conclusions and discussion

5.1. *Achievements*

In this work a new approach to subgrid modelling of passive scalar fields has been proposed. Our modelling approach is based on random kinematic velocity fields (KS) that we use as an approximation of the unknown subgrid velocity field. We couple KS to LES velocity fields by using the mean dissipation rate of the flow. The KS subgrid model fulfils our basic requirements for a model for simulating scalar variances that we set out in the introduction: it obeys Kolmogorov's inertial-range scaling, is incompressible and contains the vortical, straining and streaming regions

FIGURE 14. P.d.f.s of one separation vector component Δ_x, normalized with the mean-square separation σ_Δ for a LES+KS simulation: (*a*) p_Δ, (*b*) $\overline{p}_\Delta$, (*c*) $\overline{\overline{p}}_\Delta$. See (2.18) and (2.19) for the definitions of p_Δ, $\overline{p}_\Delta$, $\overline{\overline{p}}_\Delta$. For large time the p.d.f.s tend towards a Gaussian. Also included are data from Thomson (1990), see his figure 1, $t/(\sigma^2/\epsilon) = 0.2$ where $\sigma = u_{rms}$.

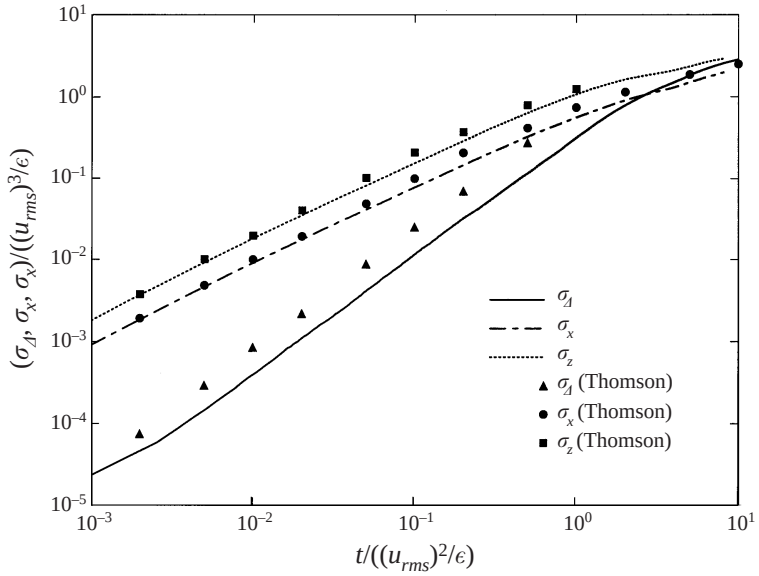

FIGURE 15. The variances of single particle dispersion σ_x and of the centre of mass of particle pairs σ_z agrees well with Thomson's model. For the variance of the mean separation of particle pairs σ_Δ we find smaller values in the inertial range in agreement with our smaller value of G_Δ. The initial separation is $\Delta_0/\eta = 1$.

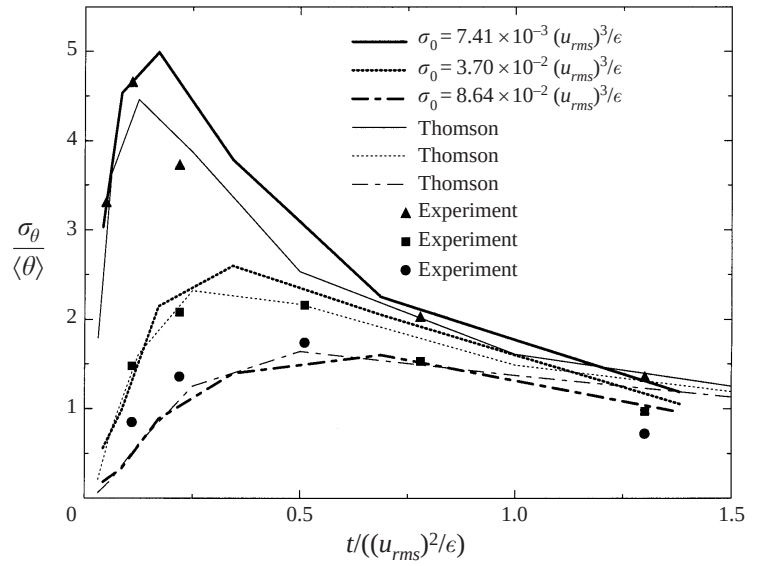

FIGURE 16. Concentration variance at the centre of a line source. Comparison with Thomson's stochastic model and experimental data from Fackrell & Robins (1982).

that exist in the small scales of turbulence. We now summarize our achievements as follows:

1. It was demonstrated that the model is able to reproduce Richardson's t^3-scaling for particle-pair dispersion over a wide range of scales and we found $G_\Delta \approx 0.07$.

2. For the first time, the p.d.f.s of the particle separation vector have been measured

in a LES with inertial-range effects explicitly resolved (and determined by the KS subgrid model). We find that the separation p.d.f. is highly non-Gaussian and becomes Gaussian for very long times. This is in agreement with Thomson's (1990) stochastic model. His model leads however to much higher absolute values of two-particle dispersion due to the random nature of the particle trajectories in his model.

3. We compute the scalar variance and base our computation on Sawford's (1983) assumptions. We validate his assumptions numerically and find (i) that the p.d.f. of single particles and the p.d.f. of the centre of mass of particle pairs are Gaussian for all times, and (ii) that the centre of mass and the particle-pair separation are statistically uncorrelated for all times.

4. Computing the variance field for an instantaneous line source where we can compare our results to experiments we find good agreement with the experiments of Fackrell & Robins (1982). Stochastic models can achieve equally good agreement provided the model parameter C_0 is chosen correctly. In our approach we do not require an input value for C_0.

5.2. *Possibilities for future improvement and development*

The kinematic modelling approach appears most natural for spectral LES because we could readily define a matching procedure at the cutoff wavenumber k_c. However, a LES defined in real space (with Smagorinsky's model, for example) could be equally coupled to the subgrid velocity field if an additional transport equation is solved for the turbulent kinetic energy. In fact, the dissipation rate is a strongly fluctuating quantity in real space and the coupling of sub- and supergrid fields by the mean dissipation rate neglects possible effects of the local variation of dissipation. However, while we couple sub- and supergrid fields via the mean dissipation rate, the modelled subgrid field itself contains eddying and straining structures which imply local variations of the dissipation rate. We therefore neglect possible correlations of such structures with the turbulent large scales. By definition, the spectral eddy viscosity (1.11) also neglects local variations of the dissipation rate (see, for example, Lesieur & Métais 1996 for a discussion on this). It would be interesting to investigate the effect of local variation of dissipation in a LES defined in configuration space.

In § 4.3 we compared our model with the eddy-diffusivity particle subgrid models that have been used in previous studies and emphasized the advantage of our model in terms of two-particle statistics. Such Brownian walk models could, in fact, be made more appropriate for two-particle statistics in the same way that Durbin (1980) and Thomson (1990) developed their stochastic models with the view to model the effect of inertial-range scaling on two-particle statistics. To our knowledge, such sophisticated stochastic models have not been used in a LES framework to date.

The accuracy of the Lagrangian integral scales is determined by the accuracy of the LES, boundary conditions and forcing schemes. It is beyond the scope of this study to investigate such effects but it is an important observation when discussing the applicability and accuracy of the kinematic subgrid model. Future work will also have to extend the ideas presented here towards more complex flows that include anisotropies and solid boundaries.

We gratefully acknowledge financial support from the Royal Society, the EPSRC (grant no. GR/K50320), the EU (contract no. ERBFMBICT96-1542) and the Gottlieb Daimler- und Karl Benz-Stiftung.

REFERENCES

Batchelor, G. K. 1952 Diffusion in a field of homogeneous turbulence. II the relative motion of particles. *Proc. Camb. Phil. Soc.* **48**, 345.

Bogucki, D., Domaradzki, J. A. & Yeung, P. K. 1997 Direct numerical simulations of passive scalars with $Pr > 1$ advected by turbulent flow. *J. Fluid Mech.* **343**, 111–130.

Borgas, M. S. & Sawford, B. L. 1996 Molecular diffusion and viscous effects on concentration statistics in grid turbulence. *J. Fluid Mech.* **324**, 25–54.

Cadot, O., Douady, S. & Couder, Y. 1995 Characterisation of the low-pressure filaments in a three-dimensional turbulent shear flow. *Phys. Fluids* **7**, 630–646.

Chollet, J. P. 1984 Two-point closures as a subgrid scale modelling for large eddy simulations. In *Turbulent Shear Flows IV* (ed. F. Durst & B. Launder). Springer.

Chollet, J. P. & Lesieur, M. 1981 Parameterization of small scales of three-dimensional isotropic turbulence utilizing spectral closures. *J. Atmos. Sci.* **38**, 2747–2757.

Ciofalo, M. 1994 Large-eddy simulation: a critical survey of models and applications. *Adv. Heat Transfer* **25**, 321–419.

Drummond, I. T., Duane, S. & Horgan, R. R. 1984 Scalar diffusion in simulated helical turbulence with molecular diffusivity. *J. Fluid Mech.* **138**, 75–91.

Durbin, P. A. 1980 A stochastic model of two-particle dispersion and concentration fluctuations in homogeneous turbulence. *J. Fluid Mech.* **100**, 279–302.

Durbin, P. A. & Hunt, J. C. R. 1980 Dispersion from elevated line sources in turbulent boundary layers. *J. Méc.* **19**, 679–695.

Egbert, G. D. & Baker, M. B. 1984 Comments on paper 'The effect of Gaussian particle-pair distribution functions in the statistical theory of concentration fluctuations in homogeneous turbulence' by B. L. Sawford (Q.J. April 1983, 109, 339–353). *Q. J. R. Met. Soc.* **110**, 1195–1199.

Elliott, F. W. & Majda, A. J. 1996 Pair dispersion over an inertial range spanning many decades. *Phys. Fluids* **8**, 1052–1060.

Fackrell, J. E. & Robins, A. G. 1982 Concentration fluctuations and fluxes in plumes from point sources in a turbulent boundary layer. *J. Fluid Mech.* **117**, 1–26.

Fung, J. C. H., Hunt, J. C. R., Malik, N. A. & Perkins, R. J. 1992 Kinematic simulation of homogeneous turbulent flows generated by unsteady random Fourier modes. *J. Fluid Mech.* **236**, 281–318.

Fung, J. C. H. & Vassilicos, J. C. 1998 Two-particle dispersion in turbulentlike flows. *Phys. Rev.* E **57**, 1677–1690.

Hadfield, M. G. 1994 Passive scalar diffusion from surface sources in the convective boundary layer. *Boundary-layer Met.* **69**, 417–448.

Heppe, B. M. O. 1998 Generalised Langevin equation for relative turbulent dispersion. *J. Fluid Mech.* **357**, 167–198.

Jiménez, J. & Wray, A. A. 1998 On the characteristics of vortex filaments in isotropic turbulence. *J. Fluid Mech.* **373**, 255–285.

Kemp, J. R. & Thomson, D. J. 1996 Dispersion in stable boundary layers using large-eddy simulation. *Atmos. Environment* **30**, 2911–2923.

Kraichnan, R. H. 1970 Diffusion by a random velocity field. *Phys. Fluids* **13**, 22–31.

Kraichnan, R. H. 1976 Eddy viscosity in two and three dimensions. *J. Atmos. Sci.* **33**, 1521–1536.

Lesieur, M. & Métais, O. 1996 New trends in large-eddy simulations of turbulence. *Ann. Rev. Fluid Mech.* **28**, 45–82.

Lesieur, M. & Rogallo, R. 1989 Large-eddy simulation of passive scalar diffusion in isotropic turbulence. *Phys. Fluids* A **1**, 718–722.

Leslie, D. C. & Quarini, G. L. 1979 The application of turbulence theory to the formulation of subgrid modelling procedures. *J. Fluid Mech.* **91**, 65–91.

Malik, N. A. 1996 Structural diffusion in 2D and 3D random flows. In *Advances in Turbulence VI* (ed. S. Gavrilakis, L. Machiels & P. Monkewitz). Kluwer.

Malik, N. A. & Vassilicos, J. C. 1999 A Lagrangian model for turbulent dispersion with turbulent-like flow structure: comparison with direct numerical simulation for two-particle statistics. *Phys. Fluids* **11**, 1572–1580.

Mason, P. J. 1992 Large-eddy simulation of dispersion in convective boundary layers with wind shear. *Atmos. Environment* **26A**, 1561–1572.

Métais, O. & Ferziger, J. 1997 *New Tools in Turbulence Modelling*. Springer.

Mydlarski, L. & Warhaft, Z. 1998 Passive scalar statistics in high-Peclet-number grid turbulence. *J. Fluid Mech.* **358**, 135–175.

Ottino, J. M. 1989 *The Kinematics of Mixing: Stretching, Chaos and Transport*. Cambridge University Press.

Pedrizzetti, G. & Novikov, E. A. 1994 On Markov modelling of turbulence. *J. Fluid Mech.* **280**, 69–93.

Pope, S. B. 1994 Lagrangian PDF methods for turbulent flows. *Ann. Rev. Fluid Mech.* **26**, 23–63.

Pumir, A. 1994 Small scale properties of scalar and velocity differences in three-dimensional turbulence. *Phys. Fluids* **6**, 3974–3984.

Richardson, L. F. 1926 Atmospheric diffusion shown on a distance-neighbour graph. *Proc. R. Soc. Lond.* A **110**, 709.

Sawford, B. L. 1983 The effect of Gaussian particle-pair distribution functions in the statistical theory of concentration fluctuations in homogeneous turbulence. *Q. J. R. Met. Soc.* **109**, 339–354.

Sawford, B. L. 1991 Reynolds number effects in Lagrangian stochastic models of tubulent dispersion. *Phys. Fluids* A **3**, 1577–1586.

Sawford, B. L. & Hunt, J. C. R. 1986 Effects of turbulence structure, molecular diffusion and source size on scalar fluctuations in homogeneous turbulence. *J. Fluid Mech.* **165**, 373–400.

Snyder, W. H. & Lumley, J. L. 1971 Some measurements of particle velocity utocorrelation functions in a turbulent flow. *J. Fluid Mech.* **48**, 47–71.

Sreenivasan, K. R. 1995 On the universality of the Kolmogorov constant. *Phys. Fluids* **7**, 2778–2784.

Sreenivasan, K. R. 1996 The passive scalar spectrum and the Obukhov-Corrsin constant. *Phys. Fluids* **8**, 189–196.

Tatarski, V. I. 1960 Radiaophysical methods of investigating atmospheric turbulence. *Izv. Vyssh. Ucheb. Zaved. 3 Radiofiz.* **4**, 551–583.

Taylor, G. I. 1921 Diffusion by continuous movements. *Proc. Lond. Math. Soc. (2)* **20**, 196–211.

Thomson, D. J. 1990 A stochastic model for the motion of particle pairs in isotropic high-Reynolds-number turbulence, and its application to the problem of concentration variance. *J. Fluid Mech.* **210**, 113–153.

Thomson, D. J. 1996 The second-order moment structure of dispersing plumes and puffs. *J. Fluid Mech.* **360**, 305–329.

Turfus, C. & Hunt, J. C. R. 1987 A stochastic analysis of the displacements of fluid elements in inhomogeneous turbulence using Kraichnan's method of random modes. In *Advances in Turbulence* (ed. G. Comte-Bellot & J. Mathieu), pp. 191–203. Springer.

Yeung, P. K. 1994 Direct numerical simulation of two-particle relative diffusion in isotropic turbulence. *Phys. Fluids* **6**, 3416–3428.

Yeung, P. K. & Pope, S. B. 1989 Lagrangian statistics from direct numerical simulations of isotropic turbulence. *J. Fluid Mech.* **207**, 531–586.